Design gridlines for passive instability suppression - Task-11 report

Hansen, Morten Hartvig; Buhl, T.

Publication date:
2006

Document Version
Publisher's PDF, also known as Version of record

Risø–R–1575(EN)

Design guidelines for passive instability suppression – Task-11 Report

M. H. Hansen and T. Buhl (RISØ)

With contributions of results from:

T. van Engelen (ECN), V. Riziotis (NTUA), E. Politis (CRES), S. Streiner (USTUTT) and H. Markou (RISØ)

Risø National Laboratory
Roskilde
Denmark
December 2006

Bibliographic Data Sheet **Risø–R–1575(EN)**

Title and author(s)

Design guidelines for passive instability suppression – Task-11 Report

M.H. Hansen and T. Buhl

Dept. or group	Date
Aeroelastic Design Wind Energy Department	December 18, 2006

Groups own reg. number(s)	Project/contract No.
1110038-00	ENK5–CT–2002–00627

Pages	Tables	Illustrations	References
55	1	27	30

Abstract (Max. 2000 char.)

In these guidelines for passive instability suppression, eight relevant topics within aeroelastic stability of turbines are considered for the parameter variations:

1. Effect of airfoil aerodynamics: The airfoil aerodynamics given by the profile coefficients for aerodynamic lift, drag, and moment are shown to have a direct effect on aerodynamic damping of blade vibrations. A redesign of the airfoils can improve the power performance of the rotor without loss of aerodynamic damping.

2. Effect of flap/edgewise frequency coincidence: The natural frequencies of the first flapwise and first edgewise blade bending modes become closer as the blades become more slender. This 1-1 resonance may lead to a coupling flap- and edgewise blade vibrations which increases the edgewise blade mode damping.

3. Effect of flap/edgewise whirling coupling: The aerodynamic damping of blade vibrations close to the rotor plane are generally lower than the aerodynamic damping of vibrations out of the rotor plane. A structural coupling between the flapwise and edgewise whirling modes can increase the overall aerodynamic damping by adding more out of plane blade motion to the edgewise whirling modes.

4. Effect of torsional blade stiffness: A low torsional blade stiffness may lead to flutter where the first torsional blade mode couples to a flapwise bending mode in a flutter instability through the aerodynamic forces.

5. Can whirl flutter happen on a wind turbine? Whirl flutter is an aeroelastic instability similar to blade flutter. Whirl flutter can occur on turbines with very low natural frequencies of the tilt and yaw modes (about 5 % of their original values).

6. Edgewise/torsion coupling for large flapwise deflections: The large flapwise deflection of modern slender blades lead to a geometric coupling of edgewise bending and torsion. The aeroelastic damping of the blade modes are affected by a flapwise prebend of the blade.

7. Effect of yaw error on damping from wake: The wake behind the rotor has an influence on the aerodynamic damping of the turbine mode due to the dynamic behavior of the induced velocities from the wake. When the turbine is operating with an yaw error, a small change in the aerodynamic damping of lower damped turbine modes is observed that may be caused by change of wake geometry.

8. Effect of generator dynamics: The total damping of turbine modes involving drivetrain rotation, as the drivetrain torsion and lateral tower modes, are highly affected by the dynamic behavior of the generator torque. The aeroelastic damping of these modes changes if the generator is operated at constant speed (e.g. asynchronous generators), constant torque, or constant power (e.g. double-fed induction machines).

ISBN

87-550-3545-0

Contents

Preface

The presented design guidelines for passive instability suppression for wind turbine are derived by the partners of the project "Aeroelastic Stability and Control of Large Wind Turbines" (STABCON) partially funded by the European Commission (EC) under the contract NNK5-CT2002-00627. The objective of passive instability suppression is to design wind turbines with enhanced aeroelastic damping of its vibrational modes during normal operation without considering the use of control actions[1].

The STABCON partners are:

- Risø National Laboratory (RISO)
- Energy Research Centre of the Netherlands (ECN)
- Centre for Renewable Energy Sources (CRES)
- National Technical University of Athens (NTUA)
- Technical University of Denmark (DTU)
- University of Stuttgart (USTUTT)
- Delft University of Technology (DELFT)
- Vestas Wind Systems A/S (VESTAS)

Several of these partners have cooperated in previous projects on aeroelastic stability of wind turbines. The STABCON project can be considered as a natural extension of at least three of those projects:

- *Stall-induced Vibrations* under EC JOULE I
- *STALLVIB* under EC JOULE III
- *DAMPBLADE* under EC Framework Programme V

It is important to note that the conclusions and recommendations of the presented guidelines are derived partly from the stability analyzes and parameter variations performed for two specific wind turbines in the STABCON project, and partly from the large amount of common knowledge and understanding on aeroelastic stability that the partners have obtained in these and other previous projects. The partners gratefully acknowledge the support by the EC, which is vital for the continuation of this successful long term research cooperation. Presently, most of the STABCON partners are cooperating in the large UPWIND project under the EC framework programme VI.

This report is written with contributions of results from other STABCON partners. The authors would especially like to thank Tim van Engelen, Vasilis Riziotis, Evangelos Politis, Kenneth Thomsen, Helen Markou, and Swen Streiner for their contributions of results, and valuable comments and suggestions in the finalization of the report.

[1] Active control is the topic of the Risø-R-1577 report "Design guidelines for integrated aeroelastic control of wind turbines – Task-12 report" [1]

1 Introduction

This report contains the design guidelines for passive suppression of aeroelastic instabilities for wind turbines. These guidelines are derived partly from stability analyzes and parameter variations conducted under Work Package 4 of the STABCON project, and partly from the partners' common knowledge and understanding of aeroelastic stability of wind turbines obtained during previous project cooperations.

The objective of WP 4 is to point out the possibilities for passive instability suppression in different turbine concepts by using new stability tools developed under the project and nonlinear aeroelastic time simulation tools[2]. This objective is achieved by first predicting the stability limits for turbines of the different concepts, then by studying the mechanisms of instability at the identified limits.

The results of stability analyzes and parameter variations conducted under WP 4 have been published internally in the Task-6 report of the STABCON project [2]. Only results that point out the main conclusions are selected for publication in this report, other results may be found in publications by the individual STABCON partners which are referenced herein when applicable.

State of the art prior to STABCON

The two wind turbine concepts that dominate the market are the Active-Stall Regulated (ASR) turbine and the Pitch-Regulated, Variable Speed (PRVS) turbine. The latter is designed to operate under attached flow conditions; whereby the risk of stall-induced vibrations is minor, whereas the ASR turbines operate under stall/separate flow conditions, which increases the prospect of stall induced vibrations, if this issue is not given attention in the design, especially of airfoils. Another instability risk exists for PRVS turbines, where the flapwise and torsional blade vibration couple in the very violent flutter instability. The continuous up-scaling of blades leads to decreased torsional stiffness and a higher risk of flutter.

Stall-regulated turbines operating with their blades in a separated flow have been known to suffer from stall-induced vibrations [3, 4]. The negative lift slope in post stall may lead to negative aerodynamic damping of blade bending modes with certain directions of vibration relative to the rotor plane [5, 6, 7, 8, 9]. The direction of blade vibration depends not only on the blade stiffness distributions and twist, but also on the turbine dynamics due to interactions of flap- and edgewise whirling modes [10, 11]. Tower modes of stall-regulated turbines may also have low, or negative damping because the blades vibrate unfavorably relative to the rotor plane. Blade vibrations close to the rotor plane, as in edgewise whirling and lateral tower modes, are most often lowest damped; but flapwise and longitudinal tower modes can also be low damped.

Pitch-regulated turbines do not operate in stall and do not suffer from stall-induced vibrations; except maybe at standstill and around rated power. The aerodynamic damping of flapwise rotor and longitudinal tower modes is high, whereas the damping of edgewise whirling, drivetrain torsion, and lateral tower modes is low due to the low aerodynamic coupling. Long slender blades operating in attached flow may have the risk of flutter if the frequency ratio between flapwise bending and torsional modes are sufficiently low and the tip speeds are sufficiently high [12, 13, 14]. The low aerodynamic damping of the drivetrain torsional modes, combined with the negative damping from the generator keeping constant power at above rated wind speeds, yield that PRVS turbines often must have active drivetrain damping built in to the controller [15].

[2] All stability and simulation tools developed and used in the STABCON project are listed in the "Final Technical Report" of the STABCON project with notes on their availability.

Test turbines

The guidelines in this report are based on hundreds of aeroelastic stability analyzes and parameter variations for the different two turbine concepts under WP 4. The two concepts are exemplified by the NM80 turbine in the original PRVS version and a fictive ASR version where a new set of operational conditions is the only modification (see Figure 1). It is clear that this simple modification does not lead to a fair comparison of the two concepts, especially because the poor stall characteristics of the rotor when it is operating in stall for the ASR turbine.

Figure 2 shows the natural frequencies and damping of the first eight aeroelastic turbine modes of the two turbines. The aeroelastic modal damping are similar until the rated wind speed of about 12 m/s, where all modes of the ASR turbine become dramatically less damped than their counterpart of the PRVS turbine. This decreased damping level is expected because of the low aerodynamic damping of blades operating in stall; the negative damping of the lateral tower bending mode, the drivetrain torsion mode, and the edgewise whirling mode is avoided on real ASR turbines by improved stall characteristics of the blade airfoils.

Outline for the guidelines

Eight relevant topics within aeroelastic stability of turbines were considered for the parameter variations in WP 4, and these topics also form the outline for the guidelines. Here is the list of topics with a brief description of their relevance:

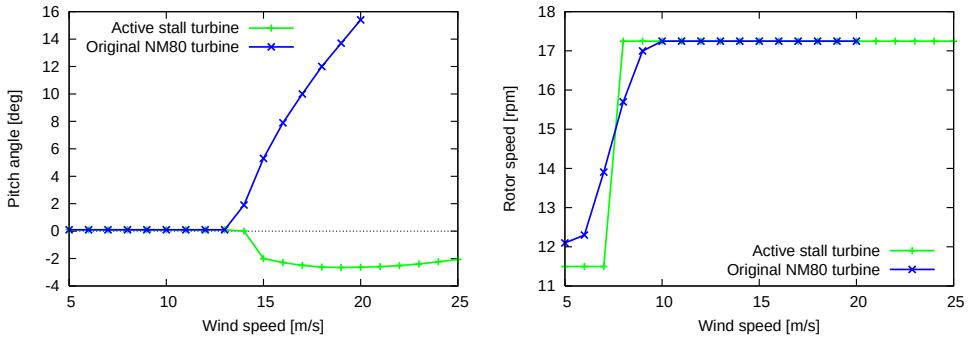

Figure 1. The pitch angles (left) and rotor speeds (right) for normal operation of the ASR and PRVS versions of the NM80 turbine.

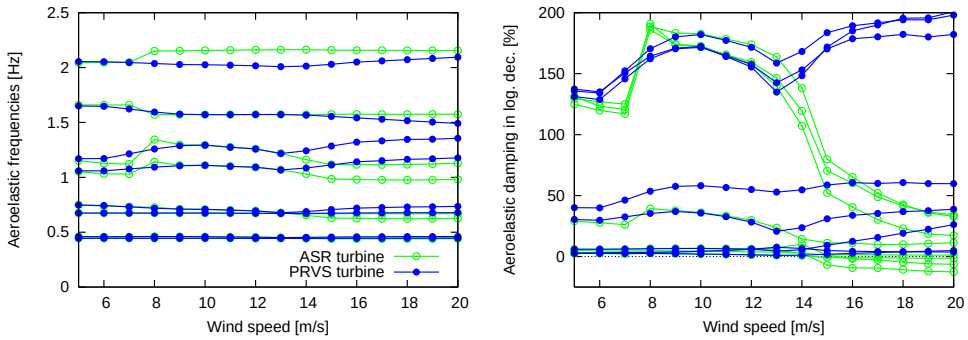

Figure 2. The natural frequencies (left) and damping (right) for the first eight aeroelastic turbine modes of the ASR and PRVS versions of the NM80 turbine. Computations performed by RISO with their aeroelastic stability tool [11].

1. **Effect of airfoil aerodynamics**
   The airfoil aerodynamics given by the profile coefficients for aerodynamic lift, drag, and moment are know to have a direct effect on aerodynamic damping of blade vibrations. It is investigated if a redesign of the airfoils can improve the power performance of the rotor without loss of aerodynamic damping.

2. **Effect of flap/edgewise frequency coincidence**
   The natural frequencies of the first flapwise and first edgewise blade bending modes become closer as the blades become more slender. It is investigated what happens when the edgewise bending stiffness distribution gradually decreases to become equal the flapwise bending stiffness distribution.

3. **Effect of flap/edgewise whirling coupling**
   The aerodynamic damping of blade vibrations close to the rotor plane are generally lower than the aerodynamic damping of vibrations out of the rotor plane. It is investigated how a structural coupling between the flapwise and edgewise whirling modes can increase the overall aerodynamic damping by adding more out of plane blade motion to the edgewise whirling modes.

4. **Effect of torsional blade stiffness**
   A low torsional stiffness of the blade may lead to flutter where the first torsional blade mode couples to a flapwise bending mode in a violent instability through the aerodynamic forces; the angle of attack change due to the torsion changes the lift in an unfavorable phase with the flapwise bending. It is investigated how the aeroelastic damping of the blade and turbine modes depend on the torsional stiffness.

5. **Can whirl flutter happen on a wind turbine?**
   Whirl flutter is an aeroelastic instability similar to blade flutter, however, the main components to the changes in angle of attack and the flapwise blade vibrations are now caused by a whirling tilt and yaw motion of the entire rotor. This instability is well-known in aeronautics [16, 17], however, few investigations have been reported for wind turbines [18]. It is investigated if whirl flutter can occur on turbines with very low natural frequencies of the tilt and yaw modes.

6. **Edgewise/torsion coupling for large flapwise deflections**
   The large flapwise deflection of modern slender blades lead to a geometric coupling of edgewise bending and torsion, where inertia and external forces in the edgewise direction yield torsional moments and deflection, and vise versa, due to the curvature of the blade. It is investigated how the aeroelastic damping of the blade modes are affected by a flapwise prebend of the blade.

7. **Effect of yaw error on damping from wake**
   The wake behind the rotor has an influence on the aerodynamic damping of the turbine mode due to the dynamic behavior of the induced velocities from the wake. When the turbine is operating with an yaw error this dynamic behavior changes. It is investigated how the aerodynamic damping of lower damped turbine modes is affected by yaw errors.

8. **Effect of generator dynamics**
   The total damping of some turbine modes like the drivetrain torsion mode and the lateral tower bending modes are highly affected by the dynamic behavior of the generator torque. It is investigated how the aeroelastic damping of the turbine modes changes if the generator is operated at constant speed (e.g. asynchronous generators), constant torque, or constant power (e.g. double-fed induction machines).

2 Effect of airfoil aerodynamics

The project called *Stall-induced Vibrations* under EC JOULE I showed the importance of the aerodynamic characteristics of the blade airfoils on the aerodynamic damping of blade vibrations [5]. Abrupt stall characteristics of the airfoils, where the lift curve has a large negative slope after the maximum lift point, may lead to stall-induced vibrations of the blades. Using computations of the work done by the aerodynamic forces on blade vibrations, the partners of this project established a method for predicting the negative aerodynamic damping leading to the stall-induced vibrations. They showed that one should avoid abrupt stall characteristics in the design of airfoils for stall-regulated turbines, and that the dynamic behavior of the airfoil aerodynamics must be taken into account when evaluating the effect of the design on the aerodynamic damping.

The STALLVIB project under EC JOULE III extended the knowledge of how the airfoil aerodynamics influences the aerodynamic damping of the blade vibrations, and furthermore showed that the direction of the blade vibrations relative to the rotor plane is an important parameter for this damping [6] (see Sections 3 and 4).

The DAMPBLADE project under EC Framework Programme V showed that the energy dissipation in the blade composite can be increased by careful lay-up design and material choice, whereby the structural damping of blade modes may compensate some of the negative aerodynamic damping [19]. The partners of the DAMPBLADE project used computations of the aerodynamic work to estimate the needed level of structural damping, however, they also developed new aeroelastic stability tools for linear eigenvalue analysis of isolated blades without the influence of the remaining turbine.

The present STABCON project under EC Framework Programme V is the natural extension of the work initiated in the previous projects. The following sections contain selected results, and main conclusions and recommendations regarding the effect of airfoil aerodynamics on the aeroelastic damping of the blade and turbine modes. These analyzes have been performed using aeroelastic stability tools developed in the STABCON project for linear eigenvalue analysis of isolated blades and entire turbines.

2.1 Selected STABCON results

An obvious effect of the airfoil aerodynamics on damping can be seen in Figure 2 in the introduction: The aeroelastic damping of the first eight turbine modes are dramatically decreased above rated wind speeds when the turbine is operating as an ASR turbine. The only difference in the two computations of aeroelastic modal damping is that the blades are operating in stall on the ASR turbine where the airfoil aerodynamics is characterized by a negative lift slope.

The partners NTUA and CRES have investigated the effect of redesigned airfoils for the outer 20 % of the blades on the aeroelastic damping of the turbine modes. The redesigns were performed with main focus on enhanced power production for both PRVS and ASR operation resulting in two new blades, one blade for each turbine concept. Calculation of the mean Weibull-weighted power performance of the different rotors showed that an increase of about 2 % was achieved for the PRVS turbine, but no significant increase was achieved for the ASR turbine.

Figure 3 shows the aeroelastic damping of the first edgewise whirling modes of the ASR and PRVS turbines with the original and new resigned blades. In the left plot, it is seen that the aeroelastic damping of these low damped modes has been increased by the redesigned blade for the PRVS operation of the NM80 turbine. In the right plot, no significant change in the aeroelastic damping of the edgewise whirling modes can be seen due to the redesigned blade for ASR operation.

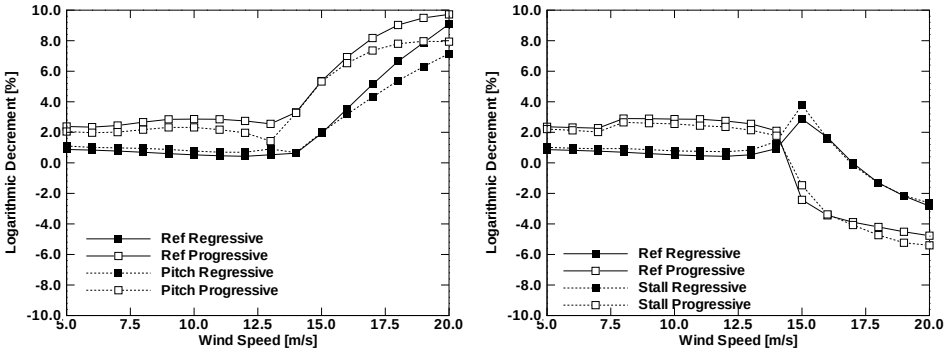

Figure 3. Aeroelastic damping of the first edgewise whirling modes of the PRVS (left) and ASR (right) turbines for different airfoils on the outer 20 % of the blades: "Ref" denotes original airfoils, and "Pitch" and "Stall" denote new airfoils for PRVS and ASR operation, respectively. Design and analysis performed by NTUA and CRES.

2.2 Conclusions and recommendations

This section contains the conclusions and recommendations with respect to the effect of airfoil aerodynamics on aeroelastic stability of PRVS and ASR turbines. It is attempted to base these conclusions and recommendations, not only on the results from the parameter variations performed in WP 4 of the STABCON project, but also on the knowledge of airfoil aerodynamics from the previous projects.

Conclusions for PRVS turbines

- The airfoil aerodynamics ensures a high damping of flapwise blade bending and longitudinal tower bending modes because the turbine operates mostly in the attached flow region of the blade airfoils where the lift is dominated by the effect of circulation yielding a linear lift curve with positive slope.
- The edgewise blade bending, drivetrain torsion, and lateral tower bending modes have low aerodynamic damping due to the low drag under attached flow conditions. Some of these modes may have negative aerodynamic damping if the blade airfoils of the turbine are operating at angles of attack close to the maximum lift.
- The modeling of unsteady aerodynamic forces on the blades has an effect on the theoretical prediction of the aerodynamic modal damping using the aeroelastic stability tools. However, the effect is minor under attached flow conditions where the unsteadiness of the aerodynamic forces is limited.

Recommendations for PRVS turbines

- The aerodynamic damping of the edgewise blade bending, drivetrain torsion, and lateral tower bending modes should be estimated from aeroelastic eigenvalue analysis using the provided tools, or from aeroelastic time simulation in cases where the aerodynamic performance of the turbine is pushed to the stall limit of the blade airfoils at around rated wind speeds.
- A redesign of blade airfoils, or a less aggressive control strategy is recommended in the case of negative aerodynamic damping.
- Careful design/choice of blade airfoils for smooth stall characteristics is still recommended due to the risk of stall-induced vibrations when the turbine is at standstill in high winds.

Conclusions for ASR turbines

- The results of the present analyzes agree with the results of the STALLVIB project under EC JOULE III [6], which showed the importance of the aerodynamic characteristics of the blade airfoils on the aerodynamic damping of the blade vibrations.
- Low aerodynamic drag combined with a negative slope of the lift curve can lead to negative aerodynamic damping of modes where the blades vibrate close to the rotor plane. This instability is called stall-induced vibrations.
- The dynamic of the entire turbine affects this direction of vibration for the blades, i.e., the actual direction of blade vibration relative to the rotor plane may be very different from the direction of vibration obtained by an isolated blade analysis.

Recommendations for ASR turbines

- For stall-regulated turbines it is always recommended to estimate the aerodynamic damping of the full turbine modes from aeroelastic eigenvalue analysis using the provided tools, or from aeroelastic time simulation.
- The stall-strips mounted on the leading edge of the blade airfoils and thereby soften their stall characteristics are commonly used in the case of negative aerodynamic damping. However, the early estimation of aerodynamic damping makes it possible to avoid stall-induced vibrations by careful design of airfoils and turbine/blade dynamics possible.

3 Effect of flap/edgewise frequency coincidence

A frequency coincidence of the first flapwise and edgewise blade bending modes may lead to a coupling of these two modes due to the 1–1 resonance, whereby the total aeroelastic blade modes will contain components of both modes. Hence, the direction of blade vibrations relative to the rotor plane will be affected by such a coincidence.

The STALLVIB project under EC JOULE III showed that the direction of the blade vibrations relative to the rotor plane is an important parameter for the aerodynamic damping of blade vibrations [6]. Using computations of the work done by the aerodynamic forces on different types of blade vibrations, the partners of the STALLVIB project showed that one should be careful in the design of the flapwise and edgewise bending stiffness distributions for the blades.

The DAMPBLADE project under EC Framework Programme V showed that the direction of vibration in the blade modes can be controlled by careful lay-up design and material choice [19]. The partners of the DAMPBLADE project used computations of the aerodynamic work and developed new aeroelastic stability tools for linear eigenvalue analysis of isolated blades to show how this aeroelastic tailoring of the blades can be done to increase the aerodynamic damping.

The present STABCON project under EC Framework Programme V is the natural extension of the work initiated in the previous projects. The following sections contain selected results, and main conclusions and recommendations regarding the effect of a gradual coincidence of flapwise and edgewise blade bending stiffness distributions on the aeroelastic damping of the blade and turbine modes. These analyzes have been performed using aeroelastic stability tools developed in the STABCON project for linear eigenvalue analysis of isolated blades and entire turbines.

3.1 Selected STABCON results

The coincidence of the natural frequencies of the flapwise and edgewise blade bending modes has been investigated by gradually reducing the edgewise stiffness distribution to become identical to the flapwise stiffness distribution.

For 100 % coincidence of the stiffness distributions, the blade is similar to a beam of isotropic and axis-symmetric cross-section, except that the mass and shear centers in blade cross-sections lie outside from the center of the neutral bending axes, whereby bending-torsion couplings slightly affect the natural frequencies and mode shapes of the bending modes. However, the free undamped natural frequencies of the first two bending modes are practically identical for 100 % coincidence. Their mode shapes are nearly unconstrained in the ratio between the flapwise and edgewise components, meaning that vibrations in one of the first two modes can easily be pushed over in the other mode. This energy transfer is based on the similarity of mode shapes, whereas the frequency coincidence leads to another type of energy transfer based on the 1–1 resonance.

This theoretical case of both frequency coincidence and mode shape similarity is quite artificial because the flapwise and edgewise stiffness distributions of real blades will not have 100 % coincidence. The natural frequencies of the first flapwise and edgewise modes may come very close, or even coincide as blades become more and more slender, but the corresponding mode shapes will be distinct, i.e., larger external disturbances are needed to push vibrations from one mode to the other. The studied coincidence of flapwise and edgewise bending stiffness distributions represents the worst case of the increasing slenderness of blades.

The effect of the flapwise and edgewise frequency coincidence on the aeroelastic stability properties of the NM80 turbine has been investigated for PRVS and ASR operation. In this section the aeroelastic damping of the blade modes obtained from isolated blade analysis are presented. The effects of the frequency coincidence on the aeroelastic damping of the full turbine modes are presented in Section 4, where the coupling of the flapwise and edgewise whirling modes due to the frequency coincidence is investigated.

Figure 4 shows the natural frequencies and damping of the first two aeroelastic bending modes of the NM80 blade for PRVS operation for different reductions of edgewise bending stiffness. For 100 % coincidence of the flapwise and edgewise stiffness distributions, the aeroelastic natural frequencies come close but they do not coincide because the structural differences in the bending-torsion couplings, and because of differences in the effects of the aerodynamic forces on the two modes.

Figure 4 shows that the aeroelastic damping of the edgewise mode (mode 2) is increased by the reduction of the edgewise stiffness, with a large increase at 100 % coincidence for wind speeds about rated. Animations of the blade vibrations show that this increased damping is caused by increased out of rotor plane motion as the flapwise and edgewise stiffness distribution gradually coincide. The cost of this increased edgewise modal damping is a reduced aeroelastic damping of the flapwise mode (mode 1); however, this mode is highly damped so the reduction will not affect the load input from this mode.

Figure 5 shows the natural frequencies and damping of the first two aeroelastic bending modes of the NM80 blade for ASR operation for different reductions of edgewise bending stiffness. The aeroelastic natural frequencies come close but they do not coincide at

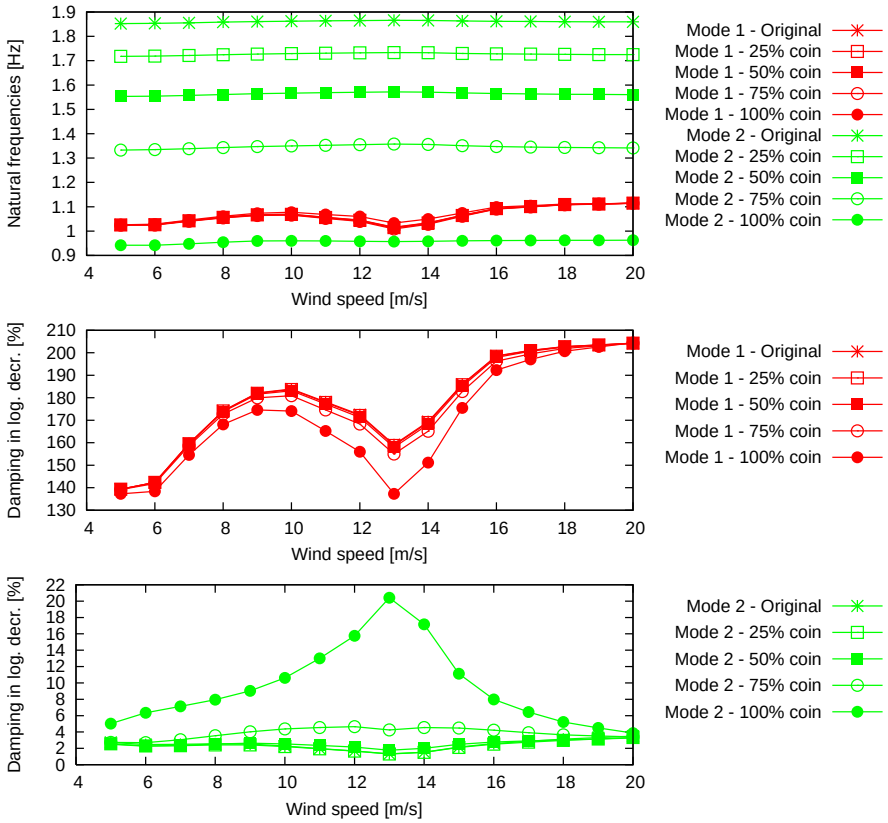

Figure 4. Aeroelastic natural frequencies and damping of the first two bending modes of the NM80 blade for PRVS operation for different reductions of edgewise bending stiffness towards coincidence with the flapwise bending stiffness distribution. Computations performed by RISO, similar results are obtained by ECN and CRES [2].

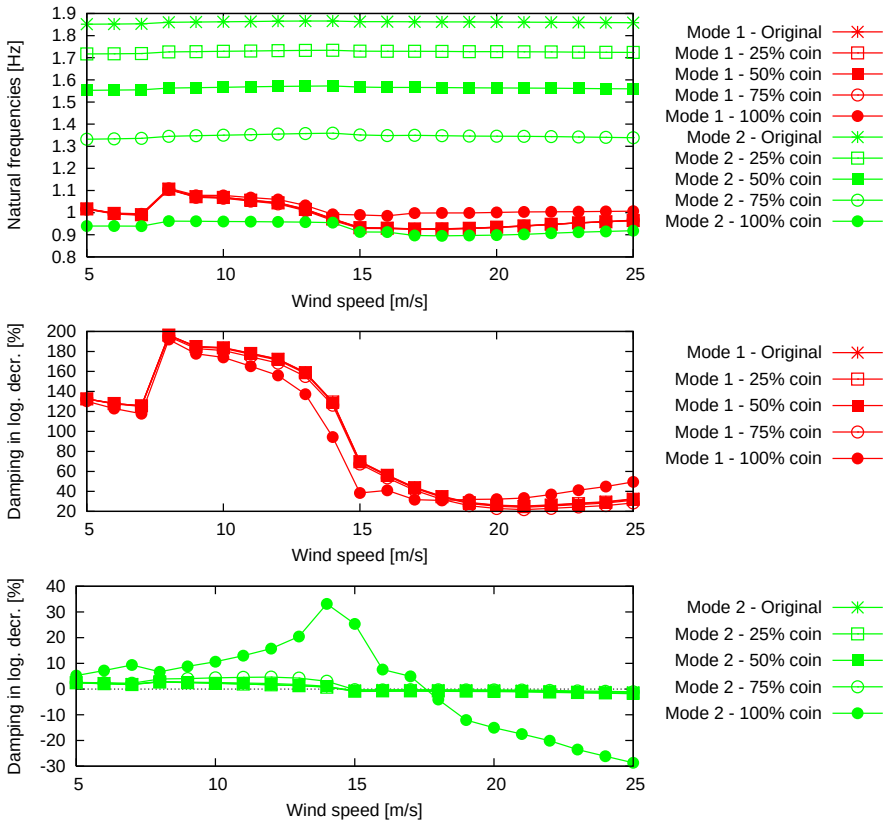

Figure 5. Aeroelastic natural frequencies and damping of the first two bending modes of the NM80 blade for ASR operation for different reductions of edgewise bending stiffness towards coincidence with the flapwise bending stiffness distribution. Computations performed by RISO, similar results are obtained by ECN and CRES [2].

100 % coincidence of the flapwise and edgewise stiffness distributions for similar reasons as for PRVS operation. The aeroelastic damping of the two modes are almost unaffected by the reduction of edgewise stiffness until the reduction to 100 % coincidence with the flapwise stiffness. Here, the damping of the edgewise mode (mode 2) is increased at wind speeds below 18 m/s but decreased above this wind speed. Similar to PRVS operation, the aeroelastic damping of the flapwise mode (mode 1) is decreased when the damping of the edgewise mode is increased, and above 18 m/s the effect of the 100 % stiffness coincidence is vise versa.

To investigate why the effect of the flapwise and edgewise stiffness coincidence on the aeroelastic modal damping chances sign around 18 m/s, it is interesting to look at the direction of blade vibrations at wind speeds below and above 18 m/s. Figure 6 shows the traces of tip motions for blade vibrations in the lowest damped edgewise modes of the original blade and the blade with 100 % stiffness coincidence for 14 m/s and 22 m/s. The traces for modal vibrations of the original blade are very similar for the two wind speeds, which agrees the almost unchanged aeroelastic damping of the edgewise mode of the original blade. The traces for the blade 100 % stiffness coincidence show a change in direction of vibration and an opening of the trace loop, which may explain the decreased aeroelastic damping above 18 m/s. Note that at 22 m/s the edgewise mode has a larger flapwise than edgewise tip amplitude, but it is still denoted as “edgewise” because the other mode has a larger flapwise-to-edgewise tip amplitude ratio.

The effect of the observed change in direction of vibration on the damping of the edgewise mode can also be seen in the work done by the aerodynamic forces on the blade when it is vibrating in this lowest damped mode. Figure 7 shows the sectional

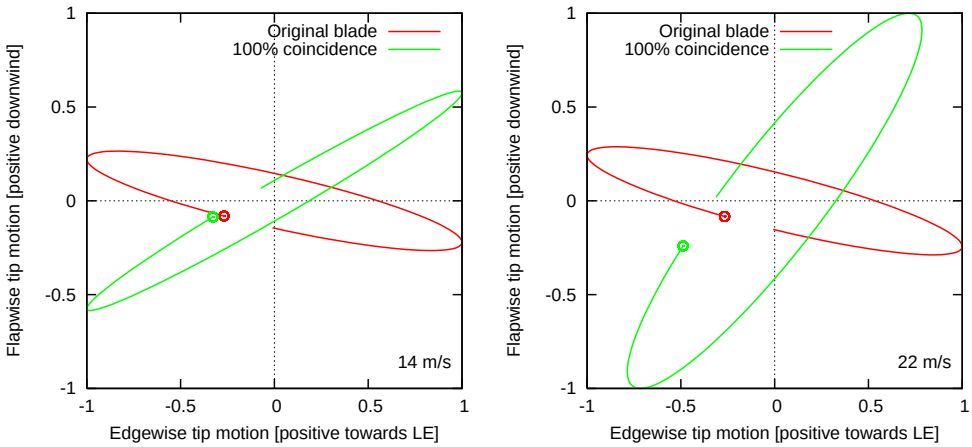

Figure 6. Traces of blade tip motion over one period of oscillation in the lowest damped blade mode at 14 m/s (left) and 22 m/s (right) of the original blade and the blade with 100 % coincidence of flapwise and edgewise stiffness distributions. The circles denote the latest position in the traces plotted from the modal amplitudes and phases given by the mode shape vector. Computations performed by RISO, similar tip traces have been provided by ECN for the flapwise and edgewise whirling turbine modes [2].

work done by linearized aerodynamic forces at 14 m/s and 22 m/s along the blade radius for vibrations in the lowest damped mode of the original blade and the blade with 100 % stiffness coincidence. The linearized aerodynamic forces are used in this computation because integrations of these aerodynamic work distributions are directly related to the aeroelastic damping obtained from the eigenvalue analysis shown in Figure 5.

The low aeroelastic damping (cf. Figure 5) and unchanged direction of vibration (cf. Figure 6) for the edgewise mode of the original blade are confirmed by low valued and similar distributions of the aerodynamic work at both wind speeds. The aerodynamic work distributions for the blade with 100 % stiffness coincidence are significantly larger and have the opposite sign at the two wind speeds, which corresponds to the change in aeroelastic damping for the edgewise mode.

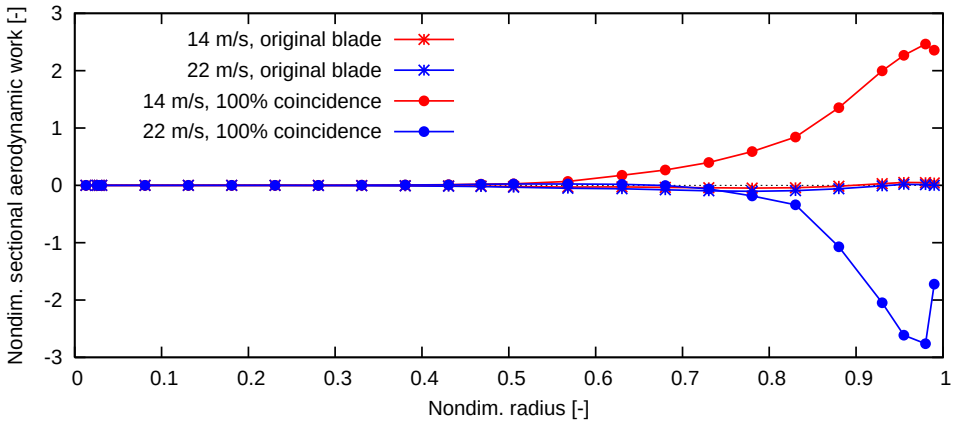

Figure 7. Sectional work done by the linear aerodynamic forces at 14 m/s and 22 m/s along the blade radius for vibrations in the lowest damped blade mode of the original blade and the blade with 100 % coincidence of the flapwise and edgewise stiffness distributions. Computations performed by RISO [2].

3.2 Conclusions and recommendations

This section contains the conclusions and recommendations with respect to the effect of frequency coincidence of the first flapwise and edgewise blade bending modes on aeroelastic stability of PRVS and ASR turbines. It is attempted to base these conclusions and recommendations, not only on the results from the parameter variations performed in WP 4 of the STABCON project, but also on the knowledge from previous projects. The frequency coincidence issue is related to the next topic in Section 4 on the effect of a flapwise and edgewise whirling coupling, wherefrom some of the following conclusions and recommendations are taken.

Conclusions for PRVS turbines

- Aeroelastic stability analyzes of the isolated blade (on a rigid hub uncoupled from the remaining turbine) show that the aeroelastic damping of the first edgewise blade bending mode is increased as the edgewise bending stiffness distribution approaches the flapwise bending stiffness distribution, whereas the first flapwise bending mode is lower, but still highly damped.
- Aeroelastic stability analyzes of the entire turbine (see Section 4) show the similar behavior: The aeroelastic damping of the first edgewise whirling modes increases due to the coupling with the first flapwise whirling modes when the flapwise and edgewise blade bending stiffness distributions become identical. The aeroelastic damping of the first flapwise whirling modes is decreased but still high.

Recommendations for PRVS turbines

- There seem to be no aeroelastic instability issues related to a coincidence of the natural frequencies of the flapwise and edgewise blade modes for a PRVS turbine. On the contrary, the frequency coincidence seem to increase the aeroelastic damping of the low damped edgewise modes due to a coupling with the flapwise modes.
- An aeroelastic eigenvalue analysis tool should be used in the case of nearly identical natural frequencies of the flapwise and edgewise blade modes, in combination with tools for nonlinear aeroelastic time simulations, for the assessment of the overall aeroelastic stability properties of the turbine.
- The aeroelastic eigenvalue analysis should be performed for the entire turbine because an isolated blade analysis may not give a similar, or conservative prediction of the effects of the frequency coincidence.

Conclusions for ASR turbines

- Aeroelastic stability analyzes of the isolated blade (on a rigid hub uncoupled from the remaining turbine) of the NM80 turbine for ASR operation show a change in the effects on the aeroelastic modal damping at high wind speeds. At low to moderate wind speeds, the aeroelastic damping of the first edgewise blade bending mode is increased, similar to effects seen for PRVS operation, when the edgewise blade bending stiffness distribution is equal to the flapwise stiffness distribution. At high wind speeds, the effect is reversed, and the edgewise mode has negative aeroelastic damping. The damping of the first flapwise blade bending mode remains positive for all reductions of edgewise stiffness.
- Aeroelastic stability analyzes of the entire turbine (see Section 4) show that the aeroelastic damping of the first edgewise whirling modes is increased for all wind

speeds when the edgewise blade bending stiffness distribution is equal to the flapwise stiffness distribution. Similar to effects seen for PRVS operation, the aeroelastic damping of the first flapwise whirling modes is decreased by the coincidence of edgewise and flapwise stiffness distributions.

- The difference in these conclusions from isolated blade analyzes and entire turbine analyzes show the complexity of the effects of the frequency coincidence: The coupling of the first flapwise and edgewise blade modes in an isolated blade analysis is based on 1–1 resonance, and in the investigated worst case also on mode shape similarity. These coupling effects will be dominating if the turbine construction is stiff or heavy, so that the blade–blade and blade–turbine interactions are minor effects. However, the structural coupling of the first flapwise and edgewise whirling modes (cf. Section 4) will dominate for the traditionally more flexible turbines, whereby the yaw and tilt components of the flapwise whirling modes may enter the edgewise whirling modes due to the reactions at the hub.
- The difference in these conclusions from isolated blade analyzes and entire turbine analyzes also indicate that the negative aeroelastic damping of the edgewise mode obtained in the isolated blade analysis may be the result of the mode shape similarity due to the stiffness distribution coincidence, and not the result of the 1–1 resonance due to the frequency coincidence.

Recommendations for ASR turbines

- There may be aeroelastic instability issues related to a coincidence of the natural frequencies of the flapwise and edgewise blade modes for an ASR turbine, where both the flapwise and edgewise modes are low damped at above rated wind speeds.
- An aeroelastic eigenvalue analysis tool should be used in the case of nearly identical natural frequencies of the flapwise and edgewise blade modes, in combination with tools for nonlinear aeroelastic time simulations, for the assessment of the overall aeroelastic stability properties of the turbine.
- The aeroelastic eigenvalue analysis should be performed for the entire turbine because an isolated blade analysis is likely not to give a similar, or conservative prediction of the effects of the frequency coincidence.

4 Effect of flap/edgewise whirling coupling

In the STALLVIB project under EC JOULE III, where the importance of the direction of blade vibrations for the aerodynamic damping of stall-regulated turbines was shown [6], the partners investigated the effect of the turbine dynamics on the low damped edgewise whirling modes. They showed that the dynamic properties of the supporting structure for the rotor (e.g. main shaft, nacelle and tower) affect the aerodynamic damping of the low damped edgewise whirling modes through the coupling of the blade vibrations to the response of the entire turbine.

The STALLVIB project initiated further investigations of the rotor whirling modes of three-bladed turbines. Petersen *et al.* showed that each blade mode of the three rotor blades can couple in two whirling modes, where the sequence of blade vibrations is forward and backward whirling relative to the rotation of the rotor [20]. They also described the rotation of the reaction forces transferred from the rotor to the supporting structure in these whirling modes, which strengthened the connection between the dynamic properties of the supporting structure and the aerodynamic damping of the whirling modes.

Thomsen *et al.* measured the aeroelastic damping of the first two edgewise whirling modes of a stall-regulated 600 kW turbine [4]. They showed that the forward whirling mode was more damped than the backward whirling mode. The two modes should have the same structural damping because their natural frequencies are similar, so the difference in total aeroelastic damping must be due to a difference in the aerodynamic damping of the two modes.

This difference in aerodynamic damping of the first forward and backward whirling edgewise modes was later explained by a difference in the effective direction of blade vibrations for the two modes [10]. The blades vibrate more out of the rotor plane in the forward whirling edgewise mode than in the backward whirling edgewise mode, because the forward whirling edgewise mode couples to the second backward whirling flapwise mode due to proximity of their natural frequencies.

With the development of aeroelastic eigenvalue analysis tools in the present STABCON project under EC Framework Programme V, these previous observations have been supported. The following sections contain selected results, and main conclusions and recommendations regarding the utilization of different couplings between edgewise and flapwise whirling modes to increase the overall aeroelastic damping of these modes. In most cases, this objective means increasing the damping of the first edgewise whirling modes without significantly reducing the damping of the first and second flapwise whirling modes.

4.1 Selected STABCON results

The first edgewise whirling modes may be coupled to the first or second flapwise whirling modes. The partners of the STABCON project have investigated the effect of both types of couplings: First, the coupling of the first flapwise and edgewise whirling modes is investigated when the edgewise blade bending stiffness is reduced to the flapwise bending stiffness. Second, the first edgewise whirling modes are coupled to the second flapwise whirling modes by two means: Reduction of the main shaft bending stiffness, and reduction of the yaw stiffness at the tower–nacelle interface.

4.1.1 Reduction of edgewise blade bending stiffness

As in Section 3, the edgewise blade bending stiffness distribution is reduced to be equal the flapwise bending stiffness distribution, whereby the effect of the coupling of the first flapwise and edgewise whirling modes due to the frequency coincidence of the corresponding blade modes was investigated.

Figures 8 and 9 show the aeroelastic natural frequencies and damping of the first forward and backward whirling flapwise and edgewise modes of the NM80 turbine under PRVS and ASR operation, respectively, for the original blade and a blade with 100 % coincidence of the edgewise and flapwise bending stiffness distributions.

For both types of operation, the natural frequencies of the edgewise whirling modes are seen to be close to the frequencies of the first flapwise whirling modes. Similar to the results of the isolated blade analyzes for PRVS operation (cf. Section 3), the low aeroelastic damping of the modes involving the first edgewise blade mode is increased, whereas the damping of the flapwise modes is decreased but still very high.

Different from the results of the isolated blade analyzes for ASR operation (cf. Section 3), the low aeroelastic damping of the modes involving the first edgewise blade mode is increased at all wind speeds due to the flapwise and edgewise stiffness coincidence. The negative aeroelastic damping obtained from the isolated blade analyzes at high wind speeds for the edgewise blade bending mode is canceled by the coupling of the first flapwise and edgewise whirling modes through the dynamics of remaining turbine. Similar to all previous results, the damping of the flapwise modes is decreased when the damping of the edgewise modes is increased, whereby the first flapwise whirling modes become negative damped at high wind speeds for ASR operation.

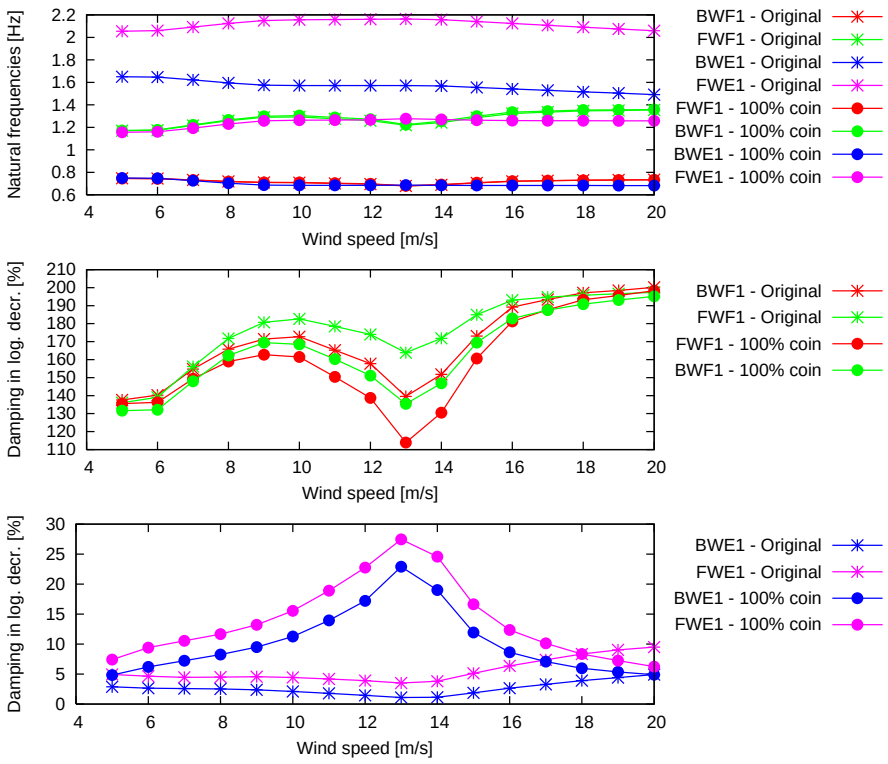

Figure 8. Aeroelastic natural frequencies and damping of the first forward and backward whirling flapwise (FWF1 and BWF1) and edgewise (FWE1 and BWE1) modes of the NM80 turbine for PRVS operation for the original blade and a blade with 100 % coincidence of edgewise and flapwise bending stiffness distributions. Computations performed by RISO, similar results are obtained by ECN and CRES [2].

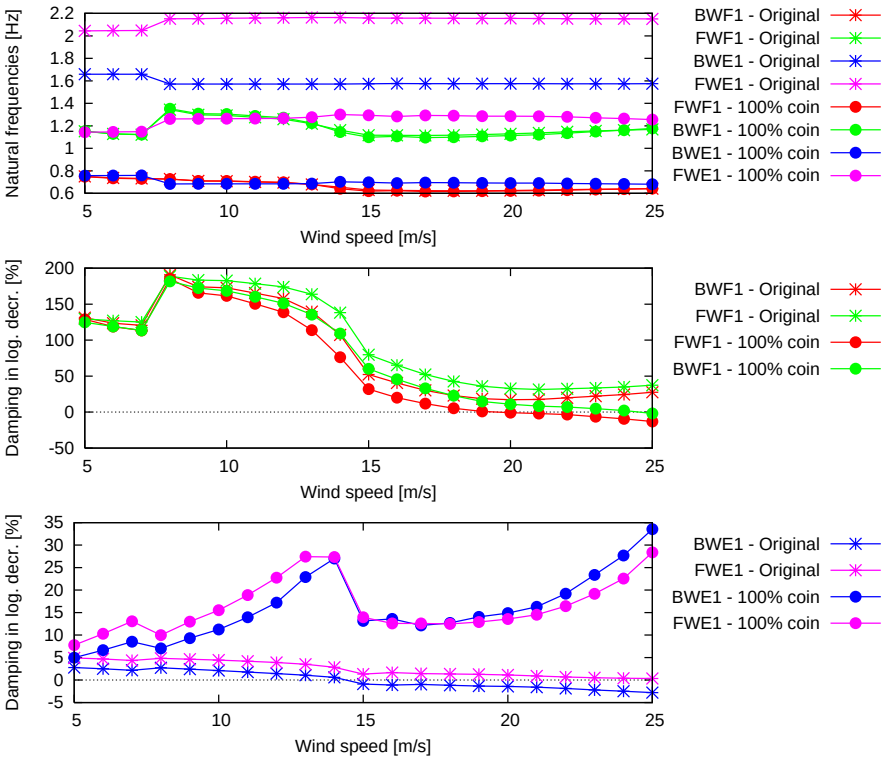

Figure 9. Aeroelastic natural frequencies and damping of the first forward and backward whirling flapwise (FWF1 and BWF1) and edgewise (FWE1 and BWE1) modes of the NM80 turbine for ASR operation for the original blade and a blade with 100 % coincidence of edgewise and flapwise bending stiffness distributions. Computations performed by RISO, similar results are obtained by ECN and CRES [2].

4.1.2 Reduction of main shaft bending stiffness

To investigate the effect of a structural coupling between the first edgewise whirling modes and the second flapwise whirling modes, the natural frequencies of the latter is lowered by reducing the bending stiffness of the main shaft to 2 % of its original stiffness. It is clear that such low bending stiffness of the shaft is not realizable, but it is a good test case for the investigations of flapwise and edgewise whirling couplings.

Figures 10 and 11 show the aeroelastic natural frequencies and damping of the first forward and backward whirling edgewise and second flapwise modes of the NM80 turbine under PRVS and ASR operation, respectively, for the original and 98 % reduced shaft bending stiffness.

For both types of operation, the natural frequencies of the second flapwise whirling modes are lowered so that the forward whirling mode lies between and the backward whirling mode lies below the first forward and backward whirling edgewise modes. It is noted that the frequencies of the flapwise and edgewise whirling modes are not so close as in the case of edgewise and flapwise blade frequency coincidence.

Figures 10 and 11 show that the aeroelastic damping of the first edgewise whirling modes is increased by the reduction of shaft stiffness under both PRVS and ASR operation. Different from the effect of the edgewise and flapwise blade frequency coincidence, the aeroelastic damping of the flapwise whirling modes is not decreased as the damping of the edgewise whirling modes is increased; on the contrary the flapwise damping seems to increase as well.

This onesided positive effect of the reduced bending stiffness indicate that the coupling

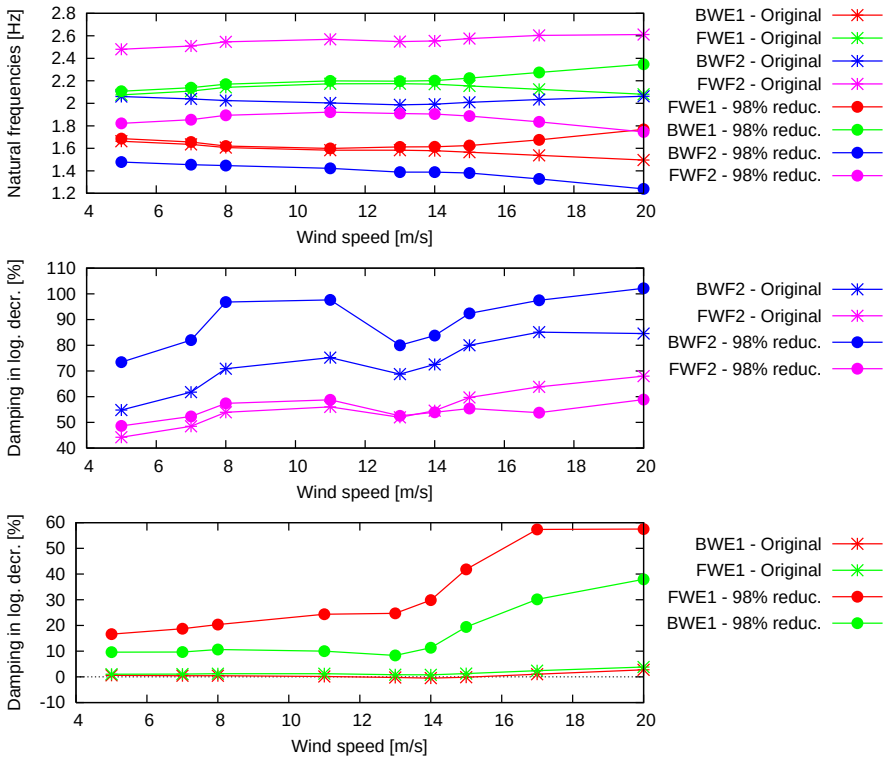

Figure 10. Aeroelastic natural frequencies and damping of the first forward and backward whirling edgewise (FWE1 and BWE1) and second flapwise (FWF2 and BWF2) modes of the NM80 turbine for PRVS operation with the original and 98 % reduced shaft bending stiffness. Computations performed by ECN, similar results are obtained by RISO and CRES [2].

of the first edgewise and second flapwise whirling modes has no dominating effect. The increased aeroelastic damping of both mode pairs may also be explained by increased out of rotor plane motion of the blades due to the increased flexibility of the shaft. Figure 12 shows this increased out of plane blade tip motion for the first edgewise whirling modes for the reduced shaft bending stiffness.

4.1.3 Reduction of yaw stiffness

To investigate the effect of a structural coupling between the first edgewise whirling modes and the second flapwise whirling modes, the natural frequencies of the latter can also be lowered by reducing the yaw stiffness at the tower–nacelle interface. In the present case, the yaw stiffness is reduced so that the frequency of the first yaw mode at standstill is lowered from 0.89 Hz to 0.05 Hz. This soft yaw case may be realizable by using highly flexible mounts for the yaw system.

Figures 13 and 14 show the aeroelastic natural frequencies and damping of the first forward and backward whirling edgewise and second flapwise modes and damping of the first tower bending modes of the NM80 turbine under PRVS and ASR operation, respectively, for the original and soft yaw stiffnesses.

Similar to the case of reduced shaft stiffness, the natural frequencies of the second flapwise whirling modes are lowered so that the forward whirling mode lies between and the backward whirling mode lies below the first forward and backward whirling edgewise modes.

For PRVS operation (cf. Figure 13), the aeroelastic damping of the edgewise whirling

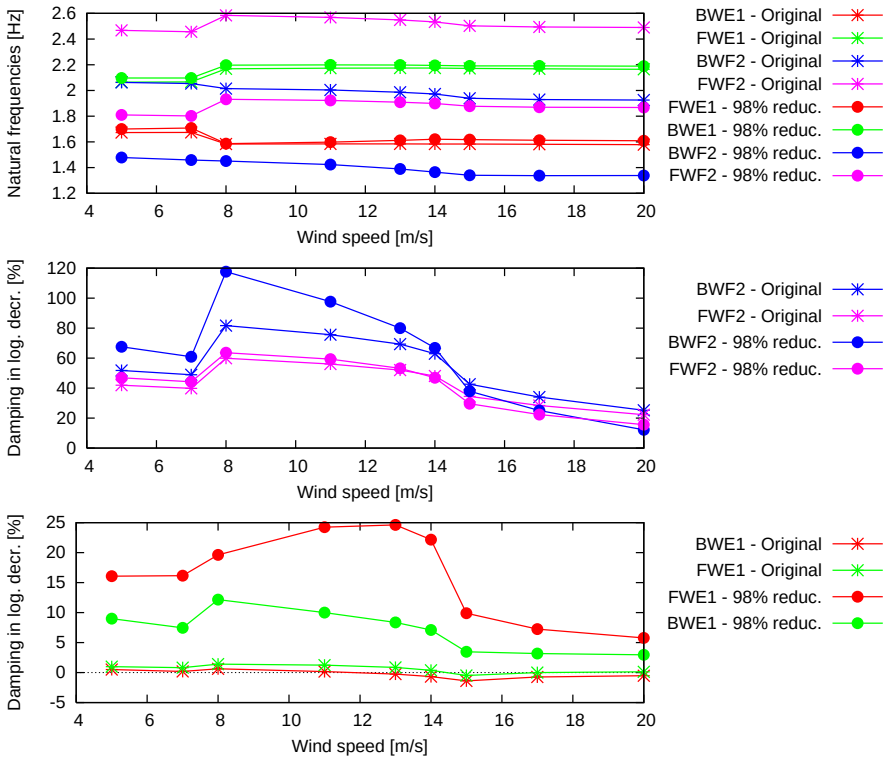

Figure 11. Aeroelastic natural frequencies and damping of the first forward and backward whirling edgewise (FWE1 and BWE1) and second flapwise (FWF2 and BWF2) modes of the NM80 turbine for ASR operation with original and 98 % reduced shaft bending stiffness. Computations performed by ECN, similar results are obtained by RISO and CRES [2].

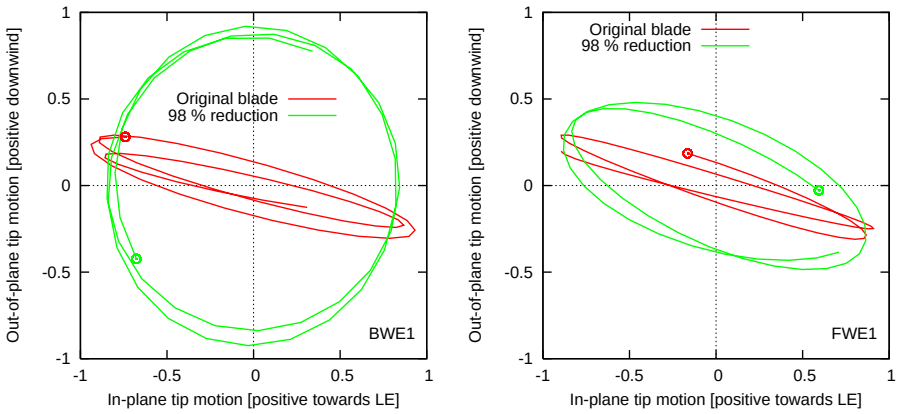

Figure 12. Traces of blade tip motion relative to the rotor plane over several period of blade oscillation in the first backward whirling (BWE1) and forward whirling (FWE1) edgewise mode of the NM80 turbine under ASR operation with original and 98 % reduced shaft bending stiffness. The circles denote the latest position in the traces plotted from the modal amplitudes and phases given by the mode shape vector. Computations performed by ECN, similar tip traces have been provided by RISO [2].

modes is increased by the soft yaw. The damping of the second backward whirling flapwise mode is also increased, whereas the forward whirling flapwise mode is almost unchanged by the soft yaw. The increased damping can be explained by more out of rotor plane vibration of the blades; more because of the lower yaw stiffness, than because of a coupling between the second flapwise and first edgewise whirling modes.

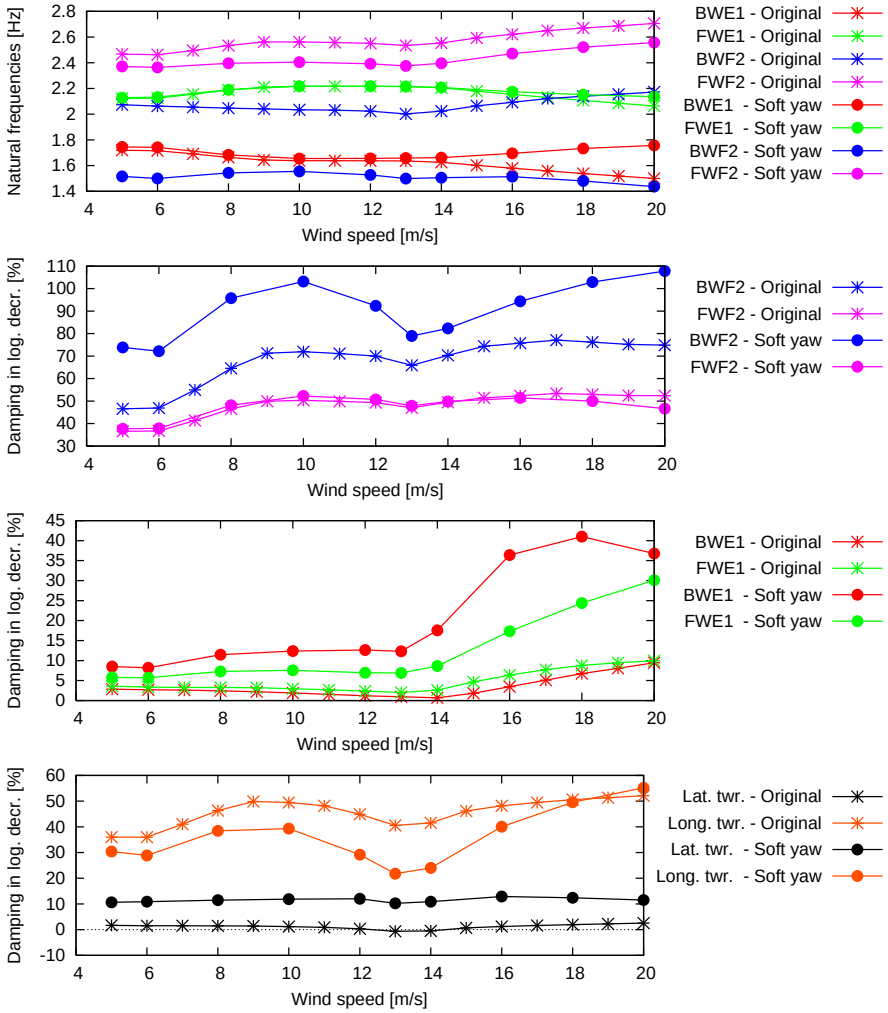

Figure 13. Aeroelastic natural frequencies and damping of the first forward and backward whirling edgewise (FWE1 and BWE1) and second flapwise (FWF2 and BWF2) modes and damping of the first tower bending modes of the NM80 turbine for PRVS operation with original and soft yaw stiffness. Computations performed by NTUA [2].

This explanation also fits with the increased damping of the lateral tower bending mode, for which the soft yaw directly leads to more out of rotor plane blade vibrations.

For ASR operation (cf. Figure 14), there is no clear damping effects of the soft yaw, except that the first lateral tower bending mode is more damped due to the more out of rotor plane blade vibrations. The longitudinal tower mode is less damped (as for PRVS operation) which may be caused by more in plane blade vibrations. For below rated wind speeds, the damping of the first edgewise and second flapwise whirling modes show the same trend as for PRVS operation due to the similarity of the operation conditions. At above rated wind speeds, in and out of rotor plane blade vibrations are almost equally low damped for ASR operation, whereby the increased out of plane vibrations has little effect on the damping.

4.2 Conclusions and recommendations

This section contains the conclusions and recommendations with respect to the effect of structural coupling of flapwise and edgewise whirling modes on aeroelastic stability of PRVS and ASR turbines. It is attempted to base these conclusions and recommen-

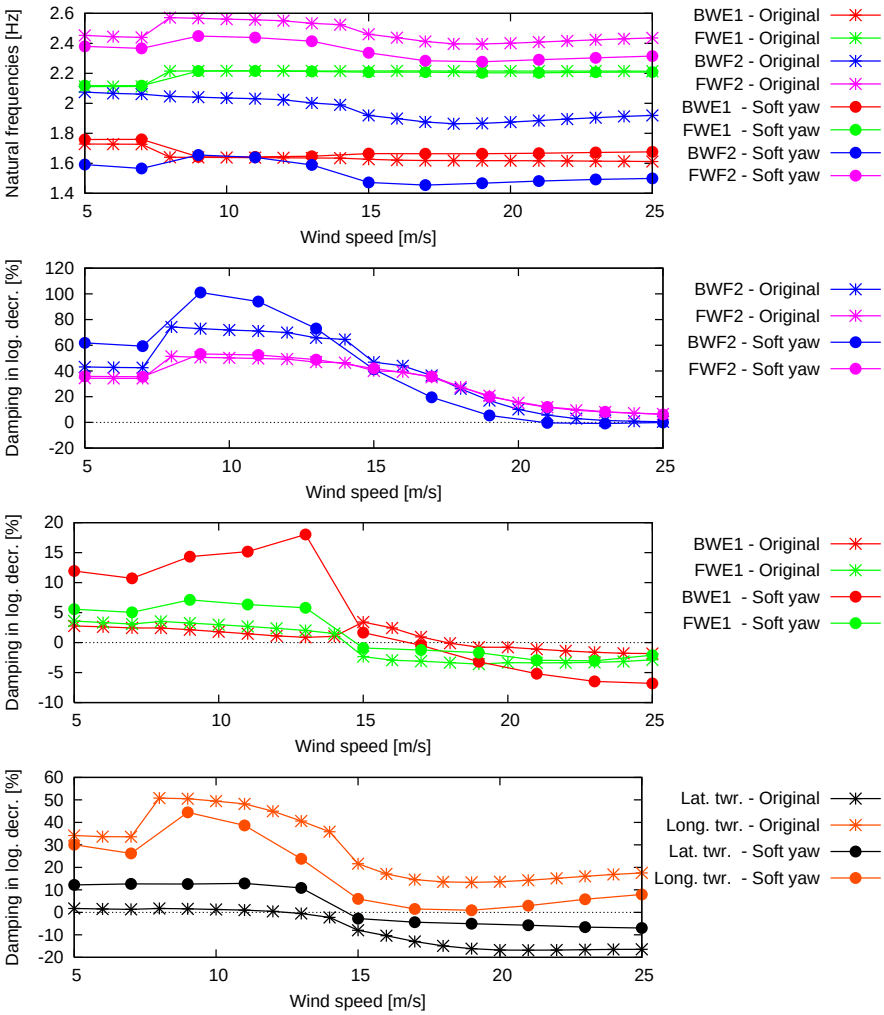

Figure 14. Aeroelastic natural frequencies and damping of the first forward and backward whirling edgewise (FWE1 and BWE1) and second flapwise (FWF2 and BWF2) modes and damping of the first tower bending modes of the NM80 turbine for ASR operation with original and soft yaw stiffness. Computations performed by NTUA [2].

dations, not only the results from the parameter variations performed in WP 4 of the STABCON project, but also on the knowledge from previous projects.

Conclusions for PRVS turbines

- A structural coupling of flapwise and edgewise whirling modes may cause the blades in an edgewise whirling mode to vibrate more out of the rotor plane and thereby obtain more aerodynamic damping, whereas the blades in a flapwise whirling mode may vibrate closer to the rotor plane and thereby loose some of its high aerodynamic damping.
- The structural coupling of the flapwise and edgewise whirling modes has an effect on the aerodynamic damping of the first tower bending modes, but it does not affect the aerodynamic damping of the turbine modes involving symmetric rotor deflection.
- The structural coupling of the flapwise and edgewise whirling modes can be obtained by tailoring e.g. the shaft bending stiffness, the tilt and yaw bending stiffness at the tower top, or the natural frequencies of the blade bending modes.

Recommendations for PRVS turbines

- A structural coupling of flapwise and edgewise whirling modes is considered to be favorable for the overall aerodynamic damping characteristics of the turbine, because the low damped edgewise whirling modes obtained higher damping on the uncritical cost of flapwise damping.
- An aeroelastic eigenvalue analysis tool for computing the turbine modal properties should be used in the tailoring of the structural coupling of the flapwise and edgewise whirling modes.
- One rule of thumb for obtaining a favorable coupling is to design the edgewise or flapwise blade stiffness such that the natural frequency of the first edgewise blade bending mode lies between the natural frequencies of the first, or second tilt and yaw modes of the turbine at standstill.

Conclusions for ASR turbines

- Similar to the PRVS turbine, a structural coupling of flapwise and edgewise whirling modes may cause the blades in an edgewise whirling mode to vibrate more out of the rotor plane and thereby obtain more aerodynamic damping below rated wind speeds, whereas the blades in a flapwise whirling mode may vibrate closer to the rotor plane and thereby loose some of its high aerodynamic damping below rated wind speeds.
- Above rated wind speeds, the flapwise whirling modes may also be low damped, and a structural coupling of the flapwise and edgewise whirling modes may not lead to an overall damping increase.
- The structural coupling of the flapwise and edgewise whirling modes has an effect on the aerodynamic damping of the first tower bending modes, but it does not affect the aerodynamic damping of the turbine modes involving symmetric rotor deflection.
- The structural coupling of the flapwise and edgewise whirling modes can be obtained by tailoring e.g. the shaft bending stiffness, the tilt and yaw bending stiffness at the tower top, or the natural frequencies of the blade bending modes.

Recommendations for ASR turbines

- A structural coupling of flapwise and edgewise whirling modes is considered to be favorable for the overall aerodynamic damping characteristics of the turbine, because the low damped edgewise whirling modes obtained higher damping on the uncritical cost of flapwise damping, except at above rated wind speeds where the damping flapwise modes can be as low, or lower than the edgewise damping.
- An aeroelastic eigenvalue analysis tool for computing the turbine modal properties should be used in the tailoring of the structural coupling of the flapwise and edgewise whirling modes.
- One rule of thumb for obtaining a favorable coupling is to design the edgewise or flapwise blade stiffness such that the natural frequency of the first edgewise blade bending mode lies between the natural frequencies of the first, or second tilt and yaw modes of the turbine at standstill.

5 Effect of torsional blade stiffness

The extensive studies of classical flutter of aircraft wings (see e.g. textbooks on aeroelasticity [21, 22]) has lead to the question if flutter also may become a problem for wind turbine blades as they become more flexible. From those studies, it is assumed that a wind turbine may have the risk of flutter if the following main criteria are satisfied:

1. The flow over the blade must be attached to ensure that nose-up (towards stall) blade torsion leads to increased lift.
2. The relative speed of the attached flow (the tip speed) must be sufficiently high to ensure sufficient energy in the aerodynamic forces.
3. The frequency ratio between a torsional mode and a flapwise bending mode must be sufficiently low for them to couple in a flutter mode.
4. The center of mass in the cross-sections on the outmost part of the blade must lie behind the aerodynamic center in a certain range to ensure the right phasing of the flapwise and torsional components of the flutter.

Other parameters such as the blade–air mass ratio, blade aspect ratio, material damping, and structural bending-torsion couplings (elastic and shear center positions) also influence the flutter limit, however, the listed criteria are the fundamental ones.

The first criterion shows that flutter may only become a problem for PRVS turbines for which the blades are operating below stall. The second criterion shows that flutter may become a problem if the tip speeds of PRVS turbines are increased. Although, the tip speed is limited by noise and load requirements, it is still interesting to investigating the case when a turbine is experiencing an overspeed.

Lobitz [12] has investigated the flutter rotor speed limit of a MW-sized wind turbine blade based on isolated blade stability analysis using quasi-steady and unsteady (Theodorsen) aerodynamics. He showed that the predicted flutter speed of the blade using quasi-steady aerodynamics is lower than the flutter speed obtained using unsteady aerodynamics. This increased flutter speed of the latter is caused by the decreased effective slope of the lift curve (cf. the first criterion) when the induced velocities from the shed vorticity is included in the modeling of the unsteady aerodynamic forces.

Lobitz [13] has furthermore investigated the effects of moving the center of mass and reducing the torsional blade stiffness on the flutter rotor speed limit of MW-sized blades using isolated blade analysis. He showed that the flutter mode for larger blades consists of the second flapwise and first torsional blade modes, and that the flutter speed limit decreases when the natural frequency ratio between these two modes is reduced (cf. the third criterion). Similar, the flutter speed limit decreases when the center of mass is moved towards the trailing edge of the blade (cf. the fourth criterion).

Hansen [14] has also investigated the effect of reduced torsional blade stiffness on the risk of flutter for a MW-sized turbine using both isolated blade and full turbine analyzes. He also found that the flutter mode consists of the second flapwise and first torsional blade modes, and that the aeroelastic damping of this flutter mode decreases when the natural frequency ratio between these two modes is reduced. The results from the isolated blade and full turbine stability analyzes for the particular turbine are similar, suggesting that isolated blade analysis is sufficient for predicting the flutter limits. This simplification is convenient, because in isolated blade analysis one does not have to solve a system with periodic coefficients.

The work by Hansen [14] is part of the early publications from the present STABCON project under EC Framework Programme V. The following sections contain selected

results from WP 4, and the main conclusions and recommendations regarding the effect of reduced torsional stiffness on the aeroelastic stability of PRVS turbines. The effect on ASR turbines has not been considered.

5.1 Selected STABCON results

The effect of reduced torsional stiffness on the aeroelastic stability of the NM80 turbine for PRVS operation has been investigated by computing the aeroelastic modal properties of the isolated blade for different relative reductions in torsional stiffness uniformly along the blade. The main focus of these analyzes has been on the risk of flutter, where isolated blade analysis is assumed to be sufficient for prediction of the flutter limits [14]. A few stability analyzes of the full NM80 turbine with reduced torsional blade stiffness has confirmed this similarity to the isolated blade analyzes.

Figure 15 shows the computed aeroelastic natural frequencies of the first six blade modes of the NM80 turbine for PRVS operation at three different wind speeds as function of the spanwise uniform reductions in torsional blade stiffness. The frequency of the first torsional mode (TS1) of the original blade (0 % reduction) is about 10.5 Hz decreases to about 2 Hz for a 90 % reduction of the torsional stiffness. The first two edgewise bending modes (LD1 and LD2) are almost unaffected by the reduced torsional stiffness. The first three flapwise modes (FL1, FL2, and FL3) are also unaffected, expect for large reductions of torsional stiffness.

Figure 16 shows the aeroelastic damping of the first torsional blade mode of the NM80 turbine for PRVS operation as function of wind speed for different reductions in torsional blade stiffness based on isolated blade analysis. The first negative damping of the torsional mode occurs for a stiffness reductions of 60 %; however, the damping is here

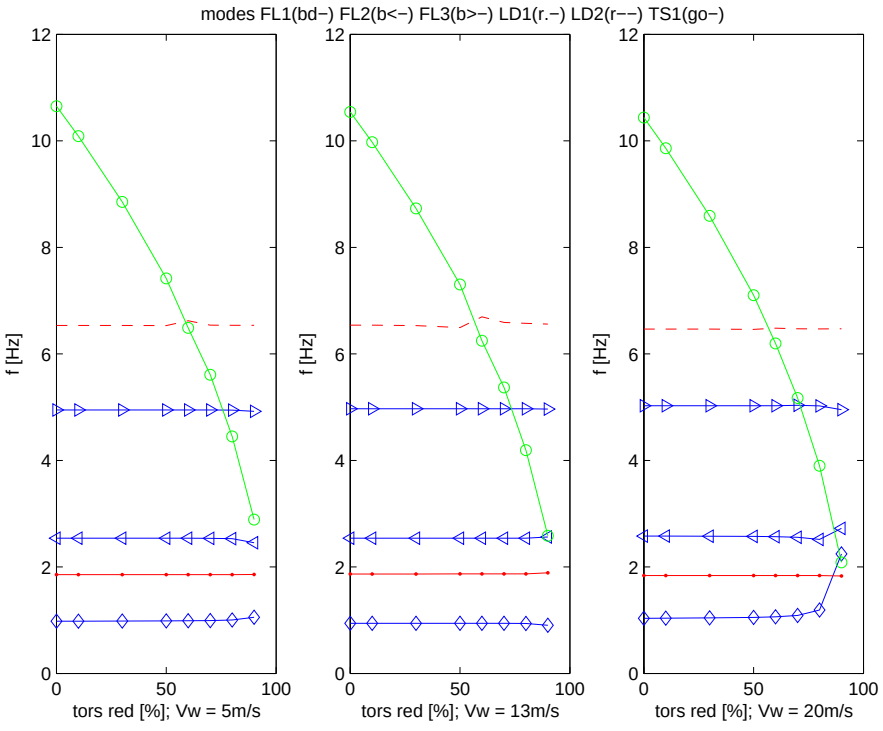

Figure 15. Aeroelastic natural frequencies of the first six blade modes of the NM80 turbine for PRVS operation at three different wind speeds as function of relative and spanwise uniform reductions in torsional blade stiffness. Computations performed by ECN, similar results are obtained by RISO [2].

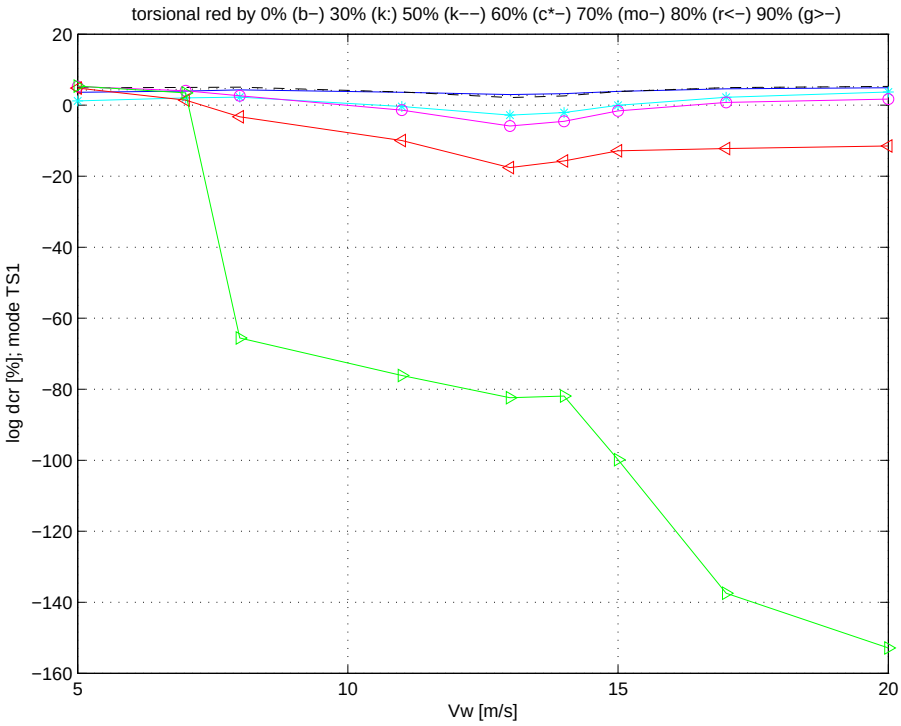

Figure 16. Aeroelastic damping of the first torsional blade mode of the NM80 turbine for PRVS operation as function of wind speed for different reductions in torsional blade stiffness. Isolated blade analysis performed by ECN, similar results are obtained by RISO [2].

only slightly negative around rated wind speed. This indicates that the instabilities for 60 % and 70 % stiffness reductions are not due to flutter, because flutter is a violent instability with highly negative damping, and it should remain at higher wind speeds where the blade is still operating in attached flow conditions.

At the torsional stiffness reductions of 80 % and 90 %, the aeroelastic damping of the first torsional mode in Figure 16 becomes highly negative and remains negative at higher wind speeds, which indicate that the instability is due to flutter. Figure 17 shows frames from an animation of a flutter mode computed in an isolated blade analysis performed by RISO with similar results as the ECN results in Figure 16. It is seen that the flutter mode contains components of the second flapwise bending and first torsional blade modes, similar to previous studies of MW-sized blades [12, 13, 14].

The reduction of the torsional blade stiffness also affects the aeroelastic damping of other blade modes. Figure 18 shows the damping of the first edgewise blade mode computed from the isolated blade with different reductions of torsional stiffness. It is seen that the damping is gradually decreased by the decreased stiffness, which may be caused by increased couplings of the edgewise bending and torsion.

Figure 17. Frames from animation of an unstable blade flutter mode consisting of the second flapwise bending and first torsional blade modes. Animation from the isolated blade analysis performed by RISO with similar results as the ECN results in Figure 16.

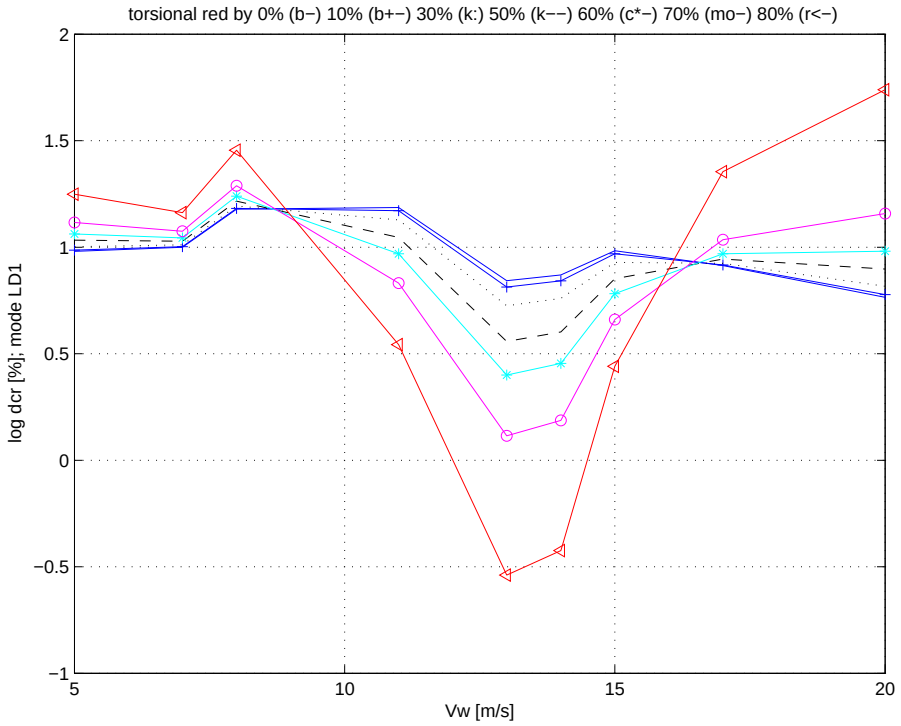

Figure 18. Aeroelastic damping of the first edgewise blade bending mode of the NM80 turbine for PRVS operation as function of wind speed for different reductions in torsional blade stiffness. Isolated blade analysis performed by ECN, similar results are obtained by RISO [2].

5.2 Conclusions and recommendations

This section contains the conclusions and recommendations with respect to the effect of reduced torsional blade stiffness on the aeroelastic stability characteristics of PRVS and ASR turbines. These conclusions and recommendations are not only based on the results from the parameter variations performed in WP 4 of the STABCON project, but also on the knowledge from previous studies [12, 13, 14].

Conclusions for PRVS turbines

- Flutter is a violent aeroelastic instability with large negative damping of the flutter mode.
- Attached flow conditions, large tip speeds, low frequency torsional stiffness, and center of mass aft in the blade cross-sections are the main criteria for flutter:
  - Flutter may occur in an overspeed situation where the tip speeds are high. Stability analyzes of medium MW-sized blades have shown a margin of a factor two from the rated rotor speed to the flutter speed [13].
  - Flutter may occur at the rated rotor speed if the torsional blade stiffness is reduced by a factor around 1/5 from the original stiffness [13, 14].
  - Flutter can not occur if the center of mass in the blade cross-sections is moved towards the leading edge in front of aerodynamic center [12, 13].
- Quasi-steady aerodynamic modeling lead to conservative predictions of flutter limits.
- Isolated blade and full turbine analyzes have shown similarities in previous flutter investigations, however, it is not proven that the coupling of the blades through the remaining turbine has no influence of the flutter limit.

- Reduced torsional blade stiffness may increase the bending–torsion coupling in an unfavorable manner that can lead to negative damping of modes involving blade bending.

Recommendations for PRVS turbines

- An aeroelastic eigenvalue analysis tool should always be used in combination with tools for nonlinear aeroelastic time simulations for the assessment of the flutter risk of large PRVS turbines, especially in overspeed situations.
- Unsteady aerodynamic modeling including the Theodorsen effect of shed vorticity is recommended for flutter analyzes because quasi-steady aerodynamics might be too conservative for optimization purposes.
- Unnecessary reduction of the torsional blade stiffness should be avoided.
- In the case of a critical reduction of torsional blade stiffness, the flutter limits can be increased by moving the cross-sectional center of mass closer to the leading edge of the blade.

Conclusions for ASR turbines

- Flutter is not a problem for stall-regulated turbines, where the blades are mostly operating under stalled flow conditions when the relative flow velocity is highest.
- Reduced torsional blade stiffness may increase the bending–torsion coupling in an unfavorable manner that can lead to negative damping of low damped modes involving blade bending.

Recommendations for ASR turbines

- In the case of reduced torsional blade stiffness, an aeroelastic eigenvalue analysis tool should be used in combination with tools for nonlinear aeroelastic time simulations for the assessment of the overall aeroelastic stability properties of the turbine.

6 Can whirl flutter happen on a wind turbine?

Whirl flutter is an aeroelastic instability known from propeller and tilt rotor aircrafts and helicopters [16, 17]. It is similar to blade flutter (cf. Section 5), however, the main components to the changes in angle of attack and the flapwise blade vibrations are here caused by a precessing tilt and yaw whirl motion of the entire rotor. The criteria that must be satisfied for whirl flutter to occur have the same elements as for blade flutter:

1. The flow over the blade must be attached to ensure that nose-up (towards stall) blade pitch leads to increased lift.
2. The relative speed of the attached flow (the tip speed) must sufficiently high to ensure sufficient energy in the aerodynamic forces.
3. The mean value of the tilt and yaw stiffness must sufficiently low to ensure the right phasing between the aerodynamic tilt/yaw moments and the backward precessing tilt/yaw whirl motion of the rotor.

Similar to blade flutter, other parameters such as the rotor–air mass ratio, blade aspect ratio, material damping, and blade bending and torsional stiffnesses also influence the flutter limit, however, the listed criteria are the fundamental ones.

The only whirl flutter analysis performed for a wind turbine known to the authors is Janetzke and Kaza's investigation of the two-bladed wind turbine MOD-2 with a teetering rotor [18]. They investigated the effect of the structural damping and the tilt and yaw stiffnesses on the risk of whirl flutter. They concluded that both structural stiffness and damping have stabilizing effects, similar to the results of propeller whirl flutter analyzes [16, 17].

In the STABCON report "Design guidelines for integrated aeroelastic control of wind turbines" [1], it is shown that high gains in the cyclic pitch controller may lead to the excitation of a backward precession whirl flutter mode. The cyclic pitch controller is used to reduce the mean tilt and yaw moments from the rotor, but it also reduces the closed loop pole frequency of the backward whirling flapwise mode corresponding to an effective stiffness reduction. The controller induced whirl flutter instability occurs when the gain is so high that the backward whirling flapwise mode has the same frequency as the first tower bending modes.

In the present STABCON report, the effect of reduced tilt and yaw stiffness on the passive aeroelastic damping of the rotor whirl modes are investigated. The following sections contain selected results from WP 4, and the main conclusions and recommendations regarding the risk of whirl flutter for PRVS turbines. Whirl flutter is not expected to be possible for ASR turbines.

6.1 Selected STABCON results

Different STABCON partners have derived simple models for prediction of whirl flutter similar to the models used in the previous studies of whirl flutter [16, 17, 18]. In the following, the mechanism and stability limits of whirl flutter are described based on such simple model (all derivations are given in Appendix A), and on nonlinear aeroelastic simulations of the NM80 turbine for PRVS operation.

To understand the mechanism of whirl flutter, the instability is analyzed by a simple two degree of freedom model of a three-bladed turbine similar to the model by Janetzke and Kaza [18] of a two-bladed turbine. The schematics of the model is shown in Figure 19, and the equations of motion are derived in Appendix A based on following assumptions:

- Blades, shaft, nacelle, and tower are rigid.
- Nacelle, shaft and rotor can tilt and yaw about a pivot point at the tower top.
- Moments of inertia for tilt and yaw about the pivot point are identical.
- Structural damping is neglected.
- The rotor is rotating at a constant speed.
- Uniform inflow to the rotor (no wind shear) and without yaw or tilt errors.
- Dynamic inflow and unsteady airfoil aerodynamic effects are neglected.
- Only variations in lift and drag due to the tilt and yaw motions are considered.

The linear equations of motion (A.4) and the linearized aerodynamic tilt and yaw moments (A.11) can be written on matrix form as

$$\begin{bmatrix} I & 0 \\ 0 & I \end{bmatrix} \begin{Bmatrix} \ddot{\upsilon} \\ \ddot{\theta} \end{Bmatrix} + \begin{bmatrix} 0 & J\Omega \\ -J\Omega & 0 \end{bmatrix} \begin{Bmatrix} \dot{\upsilon} \\ \dot{\theta} \end{Bmatrix} + \begin{bmatrix} k_\upsilon & 0 \\ 0 & k_\theta \end{bmatrix} \begin{Bmatrix} \upsilon \\ \theta \end{Bmatrix} + \begin{bmatrix} c_{11} & c_{12} \\ -c_{12} & c_{11} \end{bmatrix} \begin{Bmatrix} \dot{\upsilon} \\ \dot{\theta} \end{Bmatrix} + \begin{bmatrix} k_{11} & -k_{21} \\ k_{21} & k_{11} \end{bmatrix} \begin{Bmatrix} \upsilon \\ \theta \end{Bmatrix} = \begin{Bmatrix} 0 \\ 0 \end{Bmatrix} \quad (1)$$

where I is the moment of inertia of the nacelle and rotor for tilt and yaw about the pivot point, J is the azimuthal moment of inertia of the rotor and drivetrain, Ω is the rotor speed, k_υ and k_θ are the tilt and yaw stiffnesses at the pivot point, l is the distance from the pivot point to the rotor center, and $\dot{()} = d/dt$ denotes the time derivative.

The linearized aerodynamic tilt and yaw moments (A.11) have a symmetric part given by the aerodynamic stiffness and damping coefficients k_{11} and c_{11}, and a skew-symmetric part given by the aerodynamic stiffness and damping coefficients k_{21} and c_{12}. The coefficients depend on the air density ρ, the rotor tip radius R, the distance from the pivot point to the rotor center l, and the radial distributions of chord length c, mean relative inflow velocity U_0, mean inflow angle ϕ_0, and mean angle of attack α_0 determining the aerodynamic lift and drag coefficients and their derivatives.

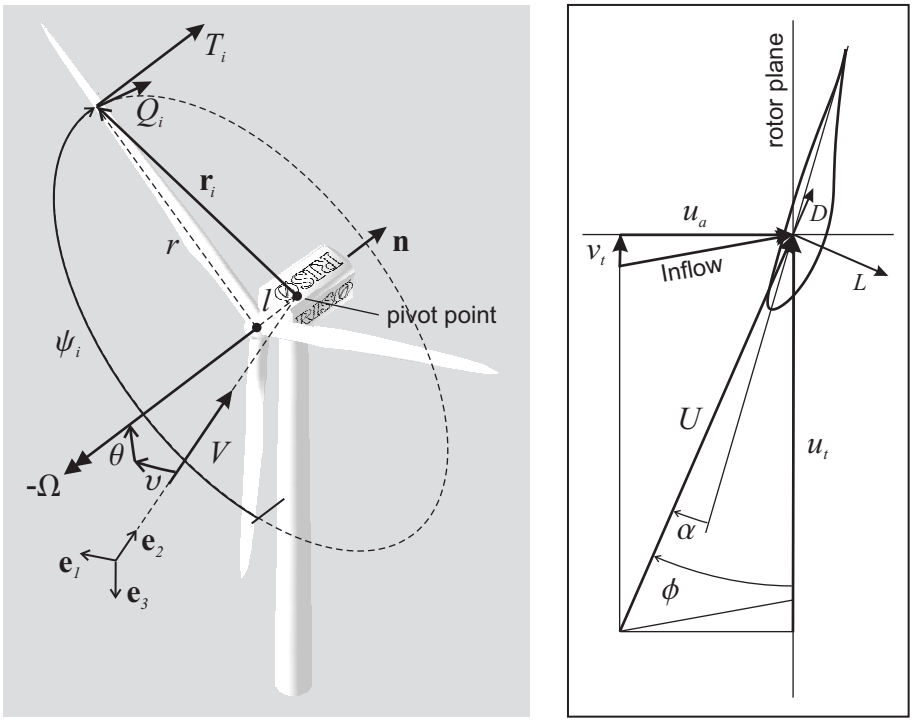

Figure 19. Schematics of the simple two degrees of freedom model of tilt θ and yaw υ motions of a three-bladed turbine rotating at a constant speed Ω (right), and the local velocity triangle at radius r on blade number i (left). Note the tangential component of the inflow v_t to the airfoil which leads to the aerodynamic stiffness terms.

As discussed in Appendix A, the symmetric stiffness coefficient is positive $k_{11} > 0$, mainly because the thrust on the rotor T has the linearized components $-2lT\theta$ and $-2lT\upsilon$ in the tilt and yaw directions. If the pivot point is placed at the rotor center $l = 0$ then the symmetric stiffness vanish $k_{11} = 0$. The skew-symmetric stiffness coefficient is positive $k_{21} > 0$ mainly because the torque on the rotor Q has the components $-Q\upsilon$ and $Q\theta$ in the tilt and yaw directions. The symmetric damping coefficient is positive $c_{11} > 0$ for attached flow on the outer part of the rotor. In fact, the symmetrical term is large for attached flow, whereby the structural damping of tilt and yaw motion will have insignificant effect on the whirl flutter limits. The skew-symmetric damping coefficient is negative $c_{12} < 0$ for attached flow on the outer part of the rotor.

To determine the stability of the equilibrium $\upsilon = \theta = 0$, the solution $\{\upsilon, \theta\}^T = \mathbf{v}e^{\lambda t}$ of a disturbance is substituted into the equations of motion (1) which leads to an eigenvalue problem with the characteristic equation

$$I^2\lambda^4 + 2Ic_{11}\lambda^3 + \left(I(k_\theta + k_\upsilon + 2k_{11}) + c_{11}^2 + (J\Omega + c_{12})^2\right)\lambda^2 + 2\big((\frac{k_\upsilon + k_\theta}{2} + k_{11})c_{11} - k_{21}c_{12} - J\Omega k_{21}\big)\lambda + (k_\upsilon + k_{11})(k_\theta + k_{11}) + k_{21}^2 = 0 \quad (2)$$

where the four zeroes are two complex conjugated pairs of eigenvalues $(\lambda_{bw}, \bar{\lambda}_{bw})$ and $(\lambda_{fw}, \bar{\lambda}_{fw})$ corresponding to backward and forward precession/whirl mode pairs. If the real part of one of these eigenvalues becomes positive, the disturbance will grow exponentially in time and the equilibrium is unstable.

Using the Routh-Hurwitz criterion (e.g. [23]) for negative real parts of all zeroes of (2), it can be shown that stability of the equilibrium is ensured if

$$\begin{aligned} a_3 = \left(\frac{k_\upsilon + k_\theta}{2} + k_{11}\right)c_{11} - k_{21}c_{12} - J\Omega k_{21} &> 0 \\ (a_1a_2 - a_0a_3)a_3 - a_1^2a_4 &> 0 \end{aligned} \quad (3)$$

where a_i are the coefficients of the characteristic equation (2). It can be shown that $(a_1a_2 - a_0a_3) >> a_1^2a_4 > 0$, whereby the whirl flutter limit can be approximated by the first of the criteria $a_3 > 0$. This inequality shows that structural and symmetric aerodynamic stiffness and damping have stabilizing effects, and that the rotor speed Ω and the moment of rotor inertia J have destabilizing effects depending on the skew-symmetric aerodynamic stiffness coefficient k_{21} (the product $k_{21}c_{12}$ is negative, however, it has a small magnitude compared to the other terms).

It is noted that the whirl flutter is almost independent of the ratio of the structural tilt and yaw stiffnesses. Furthermore, the movement of the pivot point towards the rotor center (smaller l) will have a stabilizing effect because the aerodynamic stiffness vanishes for $l = 0$. A similar conclusion holds for whirl flutter of propellers [16].

The aerodynamic coefficients are computed for the NM80 turbine at 20 m/s in Appendix A and listed in Table 1 together with other system parameters. For these parameters, the stability criterion (3) based on the simple model predicts that the equilibrium becomes unstable for an identical tilt and yaw stiffness of 2.6 MNm/rad.

This whirl flutter limit is confirmed by the left plot of Figure 20 showing the damping of the backward precessing whirl mode obtained from solution of the characteristic equation (2) for two different yaw and tilt stiffness ratios. The right plot of Figure 20 shows the damping of the backward precessing whirl mode estimated from decaying and increasing response obtained in nonlinear aeroelastic simulations of a turbine similar to the NM80 turbine at 20 m/s for the same yaw and tilt stiffness ratios. There is a good agreement between the whirl flutter limit predicted by the simple model and critical tilt and yaw stiffness seen in the simulations.

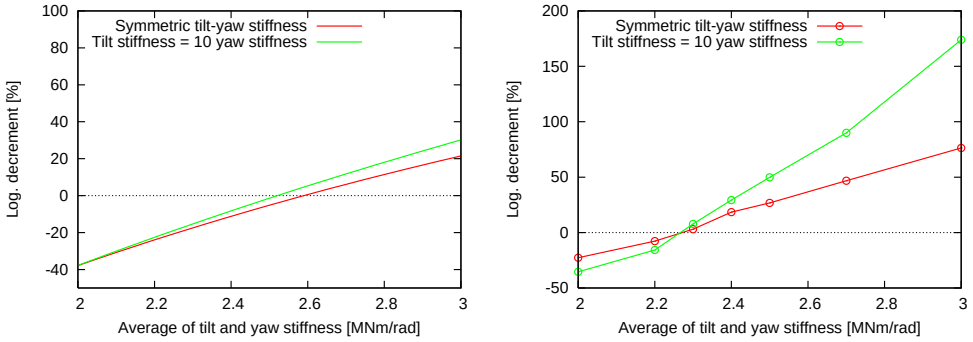

Figure 20. Aeroelastic damping of the backward precessing whirl mode of function of mean tilt and yaw stiffness obtained from solution of the characteristic equation (2) *(left plot) and estimated from decaying and increasing response obtained in nonlinear aeroelastic simulations at 20 m/s for two different yaw and tilt stiffness ratios. Computations performed by RISOE.*

To show the similarity between the simple model and nonlinear tools, the nonlinear simulations have been performed for a turbine and wind model that satisfies the listed assumptions of the simple model. Blade and shaft flexibility and the control of pitch and generator torque will influence the whirl flutter limit [16, 17, 18]. Simulations for the original NM80 turbine has shown whirl flutter for higher values of tilt and yaw stiffness, however, the critical stiffness is still not higher than 5 % of the original stiffness.

Figure 21 shows traces of the rotor center motion in backward precession whirl flutter modes with negative damping at the mean tilt and yaw stiffness $(k_\upsilon + k_\theta)/2 = 2.2$ MNm/rad and two different yaw and tilt stiffness ratios. It shows that the whirl flutter occurs in both cases, however, the motion is larger and more horizontal for the soft yaw case $k_\upsilon/k_\theta = 0.1$, as expected.

6.2 Conclusions and recommendations

This section contains the conclusions and recommendations with respect to the risk of whirl flutter for PRVS and ASR turbines. These conclusions and recommendations

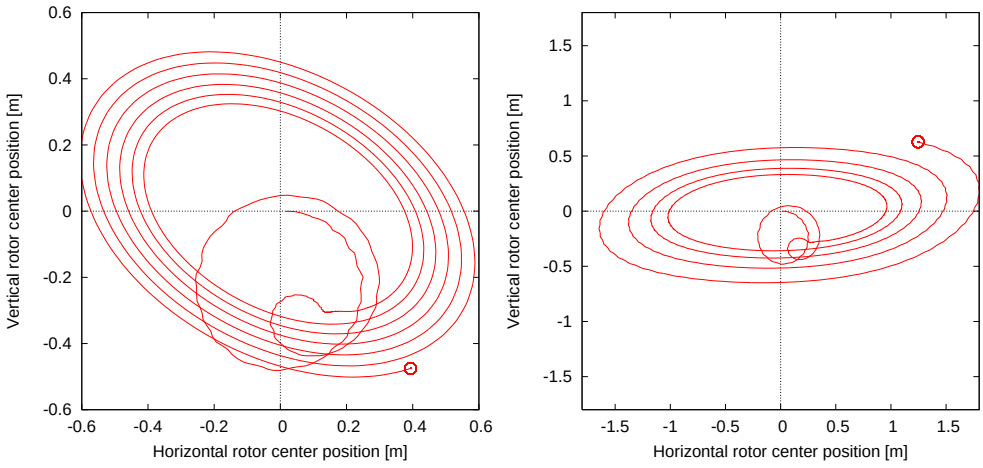

Figure 21. Traces of the rotor center motion in backward precession whirl flutter modes with negative damping at the mean structural stiffness $(k_\upsilon + k_\theta)/2 = 2.2$ MNm/rad (cf. Figure 20) with stiffness ratios $k_\upsilon/k_\theta = 1$ (left) and $k_\upsilon/k_\theta = 0.1$ (right). Nonlinear simulations performed by RISOE.

are not only based on the results from the STABCON project, but also on previous knowledge [16, 17, 18].

Conclusions for PRVS turbines

- Whirl flutter is an aeroelastic instability similar to blade flutter (cf. Section 5), where the changes in angle of attack and the flapwise blade vibrations are caused by a backward precessing tilt and yaw whirl motion of the entire rotor.
- The main criteria for whirl flutter are:
  - The flow over the blade must be attached to ensure that nose-up (towards stall) blade pitch leads to increased lift.
  - The relative speed of the attached flow (the tip speed) must sufficiently high to ensure sufficient energy in the aerodynamic forces.
  - The mean value of the tilt and yaw stiffness must sufficiently low to ensure the right phasing between the aerodynamic tilt/yaw moments and the backward precessing tilt/yaw whirl motion of the rotor.
- Whirl flutter limits of a turbine can be predicted by a simple two degrees of freedom model, however, blade and shaft flexibility and the control of pitch and generator torque will influence the whirl flutter, especially for cyclic pitch controllers [1].

Recommendations for PRVS turbines

- There is no indication of whirl flutter problems for PRVS turbine of the present size and rotor speeds, however, careful analysis is recommended in the case of cyclic pitch controllers [1].
- Whirl flutter limits can be predicted by eigenvalue analysis of simple models, by using the advanced aeroelastic stability tools developed in the STABCON project, or by using aeroelastic time simulation tools.

Conclusions for ASR turbines

- Whirl flutter is not considered to by a problem for ASR turbines.

Recommendations for ASR turbines

- Whirl flutter is not considered to by a problem for ASR turbines.

7 Edgewise/torsion coupling for large flapwise deflections

This section deals with the effect of large flapwise blade deflections on the aeroelastic damping of the low damped edgewise blade bending modes due to the nonlinear geometric coupling of edgewise bending and torsion in the case of large flapwise bending.

Previous works have studied the effects of large flapwise blade deflections on the power production and loads of MW-sized wind turbines from nonlinear aeroelastic simulations [24, 25]. These studies showed two main effects: A reduction in power production by up to 5 % due to reduced effective rotor area when the blade bend downwind and inward under the loading, and an increased pitch torque at the blade root due to the increased distance from the pitch axis to the point of action of the inplane forces on the blade.

The study of a PRVS turbine in [24] also showed that the reduced power production is compensated by the controller through the blade pitch angle settings, which causes the flapwise blade loads and tower thrust loads to increase above rated wind speeds. The effect of the increased pitch torque on the pitch actuator and its control was not considered. The study of the PRVS turbine in [25] showed that the pitch torque may be increased by up to 50 % due to the flapwise blade deflections.

Both of these previous studies have focused on the mean effects of large blade deflections and less on the dynamic effects, except that Larsen *et al.* [24] mention that the frequencies of the edgewise modes are almost unchanged by the geometric coupling with torsion due to canceling inertia and stiffness effects.

With the tools developed in the STABCON project it is possible to investigate the effects of large blade deflections on the aeroelastic stability characteristics of wind turbines. The following section contains selected results from WP 4 of the STABCON project regarding the effect of the edgewise bending/torsion coupling, due to large flapwise blade deflection, on the aeroelastic damping of the first edgewise bending mode. The main conclusions and recommendations regarding nonlinear geometric effects of large flapwise blade deflections are listed subsequent section.

7.1 Selected STABCON results

The effects of large blade deflections on the aeroelastic stability of the NM80 turbine under PRVS and ASR operation have been investigated by computing the aeroelastic modal properties of the isolated blade for different blade deflection shapes and different reductions in torsional stiffness uniformly along the blade [2].

The effects of both edgewise and flapwise deflections have been considered, however, only the effects for flapwise deflections are reported herein, because they are more significant than the effects of edgewise deflections. The flapwise deflection shape are presumed to be quadratic with a tip deflection of -4 m (upwind) or 4 m (downwind), which correspond to 10 % of the blade length.

Figure 22 and 23 show the aeroelastic damping of the first edgewise bending mode of the NM80 blade under PRVS and ASR operation, respectively, for different flapwise deflection shapes (straight blade and upwind and downwind deflected blades) and different reductions of torsional blade stiffness. It is seen that the downwind blade deflection (4 m) lead to higher aeroelastic damping of the edgewise blade mode (except at high wind speeds for PRVS operation), whereas the upwind blade deflection (-4 m) lead to lower and even negative aeroelastic damping of the edgewise blade mode. These effects become more significant when the torsional blade stiffness is reduced, which shows

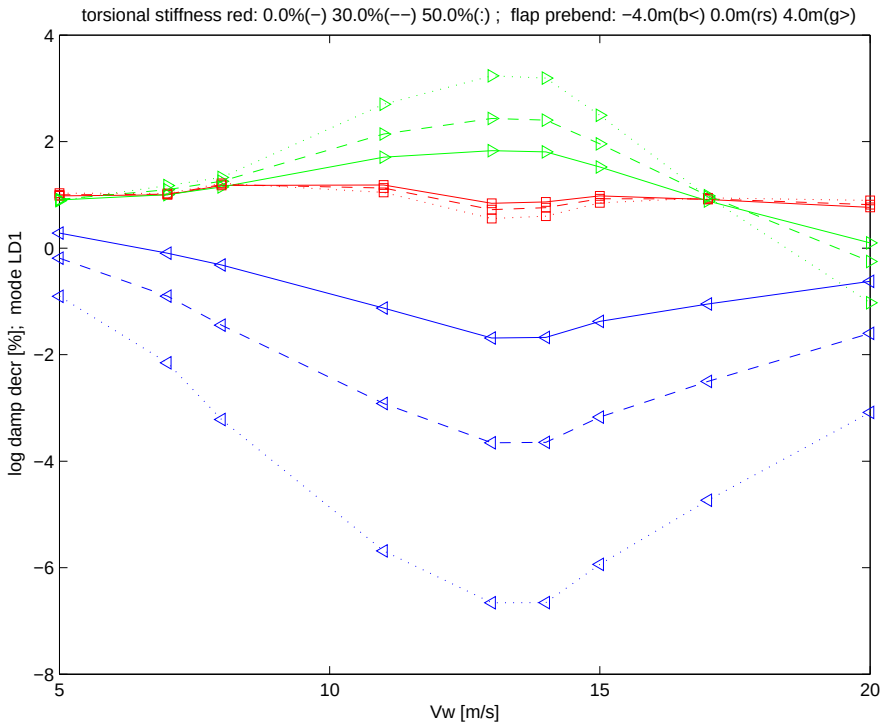

Figure 22. Aeroelastic damping of the first edgewise bending mode of the NM80 blade for PRVS operation for different flapwise deflection shapes ("flap prebend" -4 m, 0 m and 4 m refers to upwind, straight and downwind flapwise tip deflections) and different reductions of torsional blade stiffness. Computations performed by ECN [2].

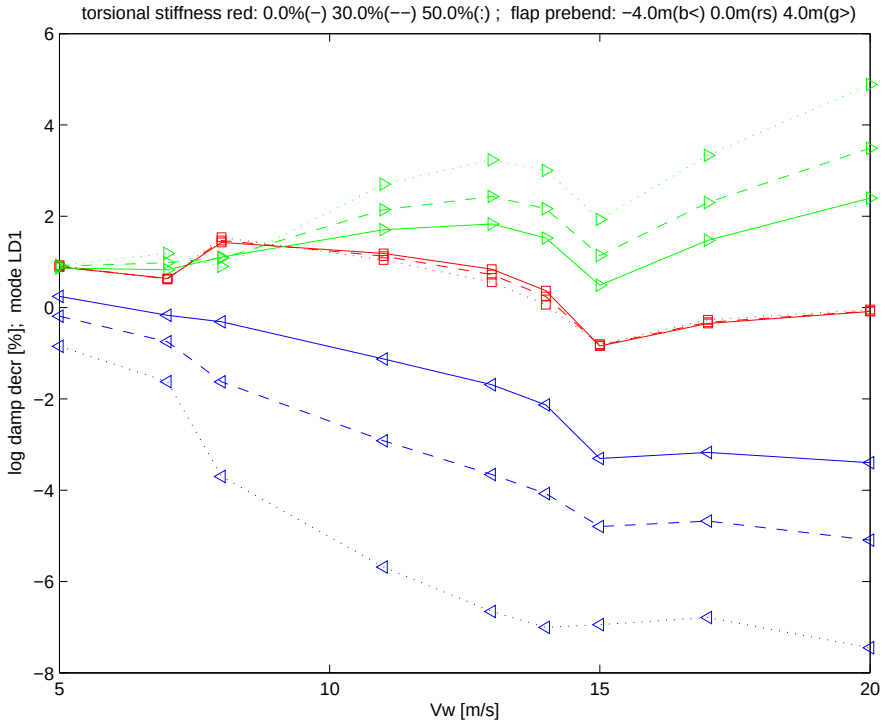

Figure 23. Aeroelastic damping of the first edgewise bending mode of the NM80 blade for ASR operation for different flapwise deflection shapes ("flap prebend" -4 m, 0 m and 4 m refers to upwind, straight and downwind flapwise tip deflections) and different reductions of torsional blade stiffness. Computations performed by ECN [2].

that the increased and decreased damping in both cases are caused by the geometric coupling of edgewise bending to torsion.

For downwind deflection, an edgewise bending in the leading-edge direction is related to blade torsion towards feathering. For upwind deflection, an edgewise bending in the leading-edge direction is related to blade torsion towards stall.

Rasmussen *et al.* [7] have investigated the effect of a coupling between translation and pitching of an airfoil on the aerodynamic damping of harmonic oscillations using an dynamic stall model. For stalled flow conditions, they found that the aerodynamic damping of a harmonic airfoil translation is increased if the airfoil is pitching towards feathering in phase with forward edgewise motion (or downwind flapwise motion), and vice versa for counter-phased pitching. Assuming similarities in the dynamic stall models, this observation explains the decreased and increased damping for upwind and downwind flapwise deflection, respectively, for ASR operation in Figure 23.

For attached flow conditions, the damping effect of the coupling between translation and pitching of the airfoil is less dominant and more dependent on the direction of translational vibration [7]. Whether the aerodynamic damping of harmonic edgewise airfoil translation is increased or decreased for in or out of phase pitching depend mostly on the direction of vibration and the modeling of the unsteady aerodynamic forces. Ignoring the small unsteady aerodynamic effects for attached flow, the increased damping for downwind flapwise deflection for PRVS operation in Figure 22 may be explained by the relative reduction of the aerodynamic loads when the blade is pitching towards feathering in forward edgewise bending. The total increase in aerodynamic loads due to the increased inflow velocities when the blade is moving forward in the edgewise mode is decreased by reduced angles of attack, except at high wind speeds where the outer part of the blade is operating at negative angles of attack. These changes in amplitude and phase in the aerodynamic load feedback to edgewise blade vibrations can explain the increased damping at moderate wind speeds, and the decreased damping at the high wind speeds.

7.2 Conclusions and recommendations

This section contains the conclusions and recommendations with respect to the effect of large blade deflections on the aeroelastic stability characteristics of PRVS and ASR turbines. These conclusions and recommendations are based on the results from the parameter variations performed in WP 4 of the STABCON project.

Conclusions for PRVS turbines

- Downwind blade deflections lead to marginally higher aeroelastic damping of the edgewise blade modes of the investigated turbine. This effect becomes more significant when the torsional blade stiffness is reduced, which shows that the increased damping is caused by the geometric coupling of edgewise bending to torsion.
- Upwind blade deflections lead to lower and even negative aeroelastic damping of the edgewise blade modes of the investigated turbine. This effect becomes more significant when the torsional blade stiffness is reduced, which shows that the increased damping is caused by the geometric coupling of edgewise bending to torsion.
- Large flapwise blade deflections affect the mean power production and loads of the turbine [24, 25]. The reduced rotor area due to inward bending of the blades may lead to decreased pitch settings above rated wind speeds to maintain rated power, whereby the flapwise blade and longitudinal tower loads are increased [24].

- Large flapwise blade deflections increase the pitch torque loads at the pitch bearing due to the increased distance from the pitch axis to the point of action of the inplane forces on the blade.

Recommendations for PRVS turbines

- The nonlinear geometric coupling of edgewise blade bending with blade torsion due to large flapwise deflections must be include in the tools used for stability and load assessments of large wind turbines.
- The nonlinear geometric effects of large blade deflections on power production and loads should be included in the structural and aerodynamic design of the blades and in the design of the pitch system.

Conclusions for ASR turbines

- Downwind blade deflections lead to higher aeroelastic damping of the edgewise blade modes of the investigated turbine. This effect becomes more significant when the torsional blade stiffness is reduced, which shows that the increased damping is caused by the geometric coupling of edgewise bending to torsion. For downwind deflections, an edgewise bending in the leading-edge direction is related to blade torsion towards feathering, which has been shown to increase the aerodynamic damping of airfoil vibrations in stalled flow [7].
- Upwind blade deflections lead to lower and even negative aeroelastic damping of the edgewise blade modes of the investigated turbine. This effect also becomes more significant when the torsional blade stiffness is reduced, which shows that the increased damping is caused by the geometric coupling of edgewise bending to torsion. For upwind deflections, an edgewise bending in the leading-edge direction is related to blade torsion towards stall, which has been shown to decrease the aerodynamic damping of airfoil vibrations in stalled flow [7].
- Large flapwise blade deflections will also affect the mean power production and loads of ASR turbines. The reduced rotor area may also be compensated by altered pitch settings that remains closer to maximum C_p above rated wind speeds to maintain rated power. The flapwise blade and longitudinal tower loads are thereby increased.
- Large flapwise blade deflections increase the pitch torque loads at the pitch bearing due to the increased distance from the pitch axis to the point of action of the inplane forces on the blade.

Recommendations for ASR turbines

- The nonlinear geometric coupling of edgewise blade bending with blade torsion due to large flapwise deflections must be include in the tools used for stability and load assessments of large wind turbines. However, it seems that the predictions of aerodynamic damping of edgewise modes, where this coupling is neglected, are conservative for blades operating in stall.
- The nonlinear geometric effects of large blade deflections on power production and loads should be included in the structural and aerodynamic design of the blades and in the design of the pitch system.

8 Effect of yaw error on damping from wake

The dynamics of the flow velocities in the rotor plane induced by the trailing wake behind the turbine (the so-called *dynamic inflow*) influences the aeroelastic stability characteristics of wind turbines [26]. This section deals the changes in aeroelastic modal damping from the wake dynamics when the turbine is operating with different yaw errors, i.e., the wind direction is not perpendicular to the rotor plane.

The DYNAMIC INFLOW project under EC JOULE I dealt with the effects and modeling of dynamic inflow based on measurements for the pitch-regulated Tjæreborg turbine [27]. Models of dynamic inflow were developed for aeroelastic time simulations, however, the effect of dynamic inflow on the aeroelastic damping was not quantified.

Madsen and Rasmussen [26] showed that the time constants of the dynamic inflow for the change of the induced velocities after a rotor load change, are important for the aeroelastic damping of turbine modes involving symmetric rotor motion. The aerodynamic damping of rotor vibrations in an axial translation (resembling the first longitudinal tower mode) and in the first flapwise blade mode, have maximal values for large time constants (a fixed wake with steady induced velocities) and reach minimal values as the time constants approach zero (fully updated wake with instant changes in induced velocities). For realistic time constants[3], the aerodynamic damping of the symmetric rotor vibrations depend on the vibration frequency, ranging from minimum damping at very low frequencies to maximum damping at high frequencies, where the dynamic inflow behaves as a fixed wake. Madsen and Rasmussen [26] showed that a model of the trailed vorticity in the near wake can be used to describe the dynamic inflow and the influence of the unsteady induced velocities on the aerodynamic damping.

For further understanding of the damping effects of the dynamic inflow, the STABCON partners have chosen to investigate the effects of yaw errors on the damping from the wake. The following sections contain selected results from WP 4 of the STABCON project and the main conclusions and recommendations regarding these effects.

8.1 Selected STABCON results

The effects of yaw errors on the aeroelastic stability of the NM80 turbine have been investigated for PRVS operation, where rotor speeds and blade pitch angles are set after the axial component of the yawed wind inflow [2]. The investigation has focused on the first tower and edgewise whirling modes which are the lowest damped modes.

Figure 24 shows the aeroelastic natural frequencies and damping of the first lateral and longitudinal tower bending modes of the NM80 turbine for 0°, 15° and 30° yaw error (rotor plane turned counterclockwise seen from above). These results are obtained from an aeroelastic eigenvalue analysis tool neglecting yaw errors, and from nonlinear aeroelastic simulations with a free wake model enabling the simulation of yawed flow, where the damping is estimated from decaying responses after each mode has been excited close to its natural frequency [28].

For both modes, the frequencies and damping from the eigenvalue analysis are lower than the damping estimated from nonlinear simulations with the free wake model for 0° yaw error. This trend of increased damping estimated from nonlinear simulations can be explained by differences in aerodynamic modeling, but it may also be caused by nonlinear effects of the aerodynamic forces when the amplitudes of blade vibrations are not infinitely small as they are in a linear eigenvalue analysis.

[3] The measurements on the Tjæreborg turbine showed that the time it takes for the induced velocities to reach a new equilibrium after a step change in pitch angle is about the time it takes for the mean wind to travel 1–2 rotor diameters [27].

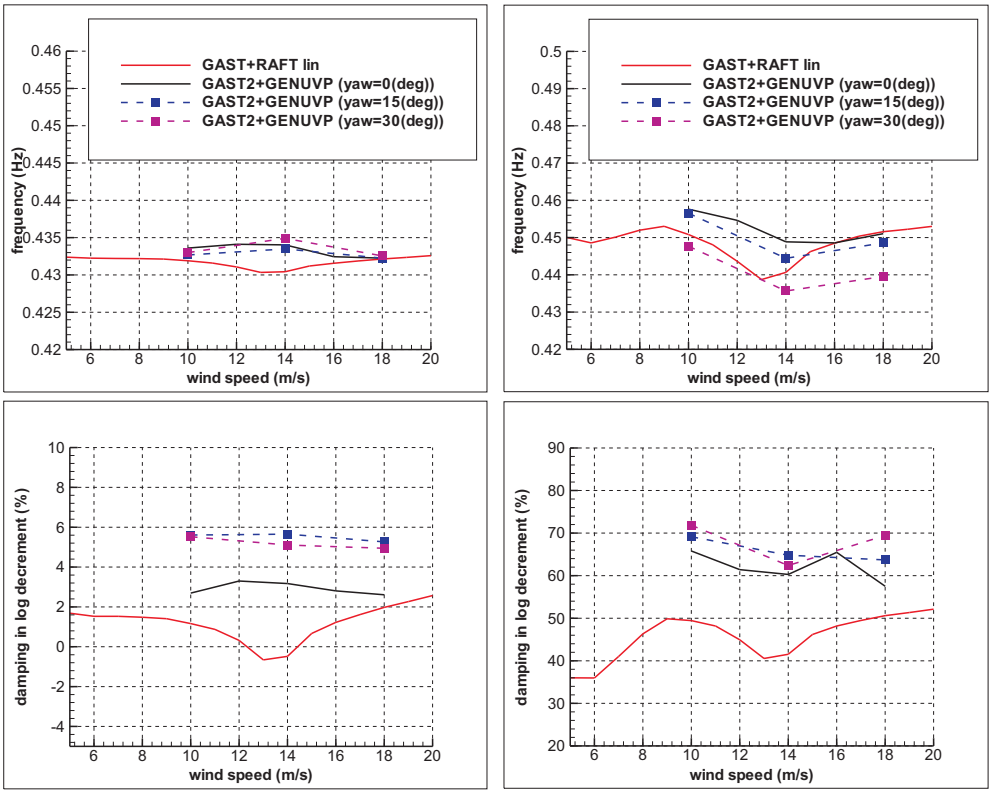

Figure 24. Aeroelastic natural frequencies and damping for 0°, 15°, and 30° yaw error of the first lateral (left) and longitudinal (right) tower bending modes of the NM80 turbine for PRVS operation obtained from eigenvalue analysis (GAST+RAFT lin) and estimated from decaying responses in nonlinear time simulations (GAST2+GENUVP). Computations performed by NTUA [2].

The estimated damping of the longitudinal tower mode is slightly increased, whereas the estimated damping of the lateral tower mode is almost doubled for 15° yaw error, but not further increased for 30° yaw error, when compared the estimated damping for 0° yaw error. There may be competing causes to this increased aerodynamic damping of the lateral mode due to the yawed inflow to the rotor.

There may be a simple geometrical explanation not related to the wake, where the misalignment of the inflow and rotor axis combined with the direction of tower vibrations of the lateral mode has a favorable damping effect. As shown in Figure 25 and seen in experimental analysis of the NM80 turbine [29], the tower is not vibrating precisely in the rotor plane for the first lateral bending mode, but in a plane that is rotated slightly counterclockwise seen from above, whereby the rotor motion obtains a wind component and thereby higher aerodynamic damping compared to motion purely in rotor plane. For the positive yaw errors, this wind component of the rotor motion and therefore the damping is increased.

This geometrical argument does however not explain why the aerodynamic damping is not further increased for the 30° yaw error. For higher yaw errors, the shape change of the wake and thereby the dynamics of its induced velocities may have more dominating effects. It is likely that the time constants for updating the induced velocities changes and become dependent of the azimuthal position of the blades, whereby the overall aerodynamic damping of the turbine modes involving rotor motion change.

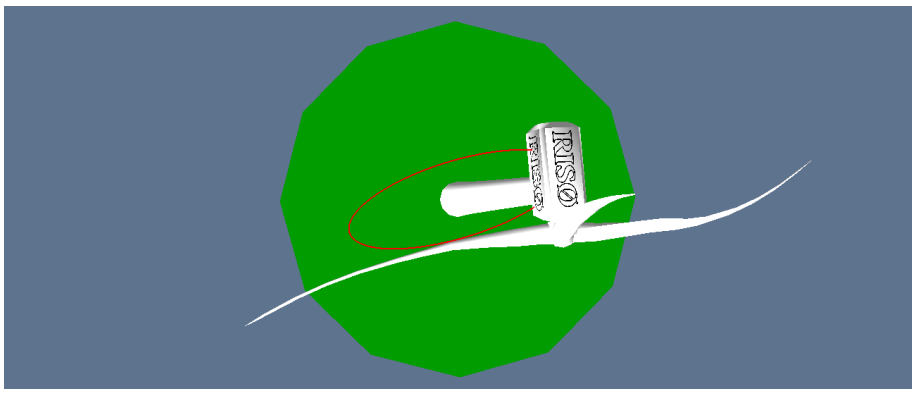

Figure 25. Trace of skew tower top motion in the first structural (no aerodynamic forces) lateral tower bending mode at rated rotor speed due to gyroscopic rotor forces and coupling with blade deflections and drivetrain torsion. Animation by RISOE.

8.2 Conclusions and recommendations

This section contains the conclusions and recommendations with respect to the effect of the trailing wake on the aeroelastic stability characteristics of PRVS and ASR turbines. These conclusions and recommendations are not only based on the results from the STABCON project, but also on previous knowledge [26].

Conclusions for PRVS turbines

- Dynamic inflow (dynamics of velocities induced by the trailing wake) has a destabilizing effect on the aerodynamic damping of turbine modes involving axial rotor vibrations [26].
- This destabilizing effect on the aerodynamic damping of axial rotor vibrations depend on the frequencies of the vibrations relative to the time constants in the updating of induced velocities.
- As rule of thumb, the induced velocities are updated in the time it takes the mean wind to travel 1–2 rotor diameters after a step change in rotor loading.
- Aerodynamic damping of tower modes are changed by yawed inflow to the rotor.

Recommendations for PRVS turbines

- Dynamic inflow should be included in aeroelastic stability tools and nonlinear simulation tools used for assessment of turbine stability and loads.

Conclusions for ASR turbines

- Similar to PRVS turbines, the dynamic inflow will have a destabilizing effect on the aerodynamic damping of turbine modes involving axial rotor vibrations [26]. However, the effect will be less dominant because the variations in rotor loads, and thereby also in induced velocities, due to the vibrations will be smaller in stall.

Recommendations for ASR turbines

- Dynamic inflow should be included in aeroelastic stability tools and nonlinear simulation tools used for assessment of turbine stability and loads.

9 Effect of generator dynamics

Asynchronous generators (short-circuited induction machines) used for ASR turbines are operating at a constant speed determined by the torque through the relation between the *slip* and torque. The slip $s = (p\omega - \omega_e)/\omega_e$ is the relative difference between the generator speed ω and the angular grid frequency ω_e/p, where p is the number of pole pairs in the generator. Commonly, the asynchronous generators of ASR turbines can be operated at two different speeds by switching pole pairs on and off, thereby changing the angular grid frequency.

Doubly-fed induction generators (DFIGs) used for PRVS turbines are operating at variable speeds due to the control of the effective angular grid frequency by frequency converters. Commonly, the objective of the controller may either be to hold a constant torque T_0, or to hold a constant power P_0.

Detailed modeling of generator dynamics to investigate the electrical conditions under for example grid failure require complex models solved at high sampling frequencies. However, for aeroelastic simulations in assessment of turbine stability and loads, it is sufficient to include the low frequency dynamics of short-circuited and doubly-fed induction generators using reduced order models (see e.g. [30]).

General conclusions on the effects of the different generator types on the damping of rotational drivetrain vibrations can be deduced from linear quasi-steady modeling of the generator speed-torque relationships for the different types:

Asynchronous generator:	$T_g = T_0 + \alpha\,\omega$	Positive damping
DFIG - constant torque:	$T_g = T_0$	Zero damping
DFIG - constant power:	$T_g = T_0 - \frac{P_0}{\omega_0^2}\,\omega$	Negative damping

where $\alpha > 0$ is the positive slope of torque-speed curve of the asynchronous generator, and ω_0 is the generator speed at the linearization point. The drivetrain damping from asynchronous generators is positive because higher generator speed leads to higher counter torque. The drivetrain damping from DFIGs controlled to hold constant torque is zero because there is no relationship between speed and torque. The drivetrain damping from DFIGs controlled to hold constant power is negative because higher generator speed leads to lower counter torque.

With the development of aeroelastic eigenvalue analysis tools in the present STABCON project, it is possible to investigate the effect of the different generator dynamics on the overall aeroelastic damping of the turbine modes, especially modes involving drivetrain rotations such as the drivetrain torsional modes, and the lateral tower bending modes. The following sections contain selected results, and main conclusions and recommendations regarding the damping effects of asynchronous and doubly-fed induction generators on the modes of PRVS and ASR turbines, and thereby the effect on the aeroelastic stability limits of the turbines.

9.1 Selected STABCON results

The effect of generator dynamics on the aeroelastic stability characteristics of PRVS and ASR turbines depend on the generator type. As mentioned in the introduction, the ASR turbines have asynchronous generators which operate at constant speed with high rotational drivetrain damping due to the positive slip-torque slope. The modes of ASR turbines that have a significant component of drivetrain rotation will therefore have increased damping due to this generator slip damping.

The PRVS turbines have doubly-fed induction generators (DFIGs) with constant torque or power control, where constant power control leads to negative rotational drivetrain damping due to the inverse proportionality of speed and torque. The modes of PRVS turbines that have a significant component of drivetrain rotation will therefore have decreased damping if the DFIG controller holds constant power instead of torque.

When the generator torque is kept constant, the drivetrain has free-free torsional boundary conditions, whereas the constant generator speed of an asynchronous generator corresponds to a fixed-free drivetrain. As part of the investigations of the effects of generator dynamics on the modal turbine damping, an aeroelastic stability analysis of the NM80 turbine in PRVS operation has been performed for three different models of the generator: Constant speed (fixed-free), constant torque (free-free), and constant torque with a damping feedback, where an overspeed (relative to a reference speed) leads to an increase of the torque.

Figure 26 shows the aeroelastic natural frequencies and damping of the first torsional drivetrain and lateral tower bending mode of the NM80 turbine in PRVS operation for the three different generator models. There is a large increase of the natural frequency of the torsional drivetrain mode (and a small increase for the lateral tower frequency) because the boundary conditions of the drivetrain change from fixed-free to free-free.

The damping of the torsional drivetrain mode is decreased and becomes more independent of wind speed as the generator model is changed from constant speed to constant torque. The reduced damping may be caused by the change in aerodynamic damping due to the change of frequency, or because the modal mass normalized amplitude of the rotor rotation and thereby the coupling to aerodynamic forces is smaller for a free-

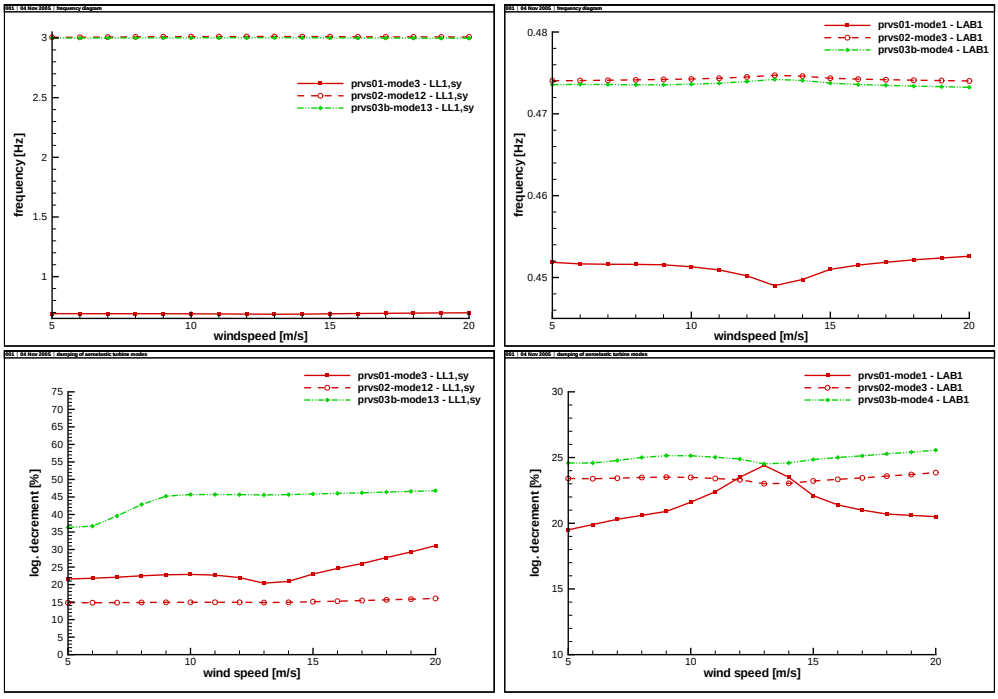

Figure 26. Aeroelastic natural frequencies (top) and damping (bottom) of the first torsional drivetrain mode (left) and first lateral tower bending mode (right) of the NM80 turbine in PRVS operation for three different generator models: Constant generator speed (fixed-free drivetrain denoted "PRVS01"), constant generator torque without damping feedback (free-free drivetrain denoted PRVS02), and constant generator torque with damping feedback (free-free drivetrain with damping denoted PRVS03b). Computations performed by USTUTT, similar results have been obtained by ECN [2].

free torsional drivetrain mode. The damping feedback added to the generator torque leads to increased damping of the torsional drivetrain mode, however, it also leads to variations in power.

The effect of the different generator models on the damping of the lateral tower mode is similar to the effect on the drivetrain damping, because the lateral tower mode is coupled with drivetrain rotation due to the rolling of the tower top in the lateral bending. The changes of damping are not so large because the drivetrain rotation amplitude in the lateral tower mode is much lower.

9.2 Conclusions and recommendations

This section contains the conclusions and recommendations with respect to the effect of generator dynamics on the aeroelastic stability characteristics of PRVS and ASR turbines. These conclusions and recommendations are not only based on the results from the STABCON project, but also on prior knowledge.

Conclusions for PRVS turbines

- Doubly-fed induction generators are used for variable speed operation of PRVS turbines, whereby free-free boundary conditions apply for the drivetrain torsion in combination with either constant torque or power control of the generator torque.
- For a PRVS turbine using a constant torque control strategy, the doubly-fed induction generator adds no damping to modes involving drivetrain torsion, e.g. collective rotor modes and tower bending modes.
- For a PRVS turbine using a constant power control strategy, the doubly-fed induction generator adds negative damping to modes involving drivetrain torsion, e.g. collective rotor modes and tower bending modes.

Recommendations for PRVS turbines

- An aeroelastic stability tool that includes the negative damping of drivetrain rotational vibrations in the case of constant power control of the doubly-fed induction generator should be used in the assessment of the aeroelastic stability limits of PRVS turbines.

Conclusions for ASR turbines

- Asynchronous generators are used for constant speed operation of ASR turbines, whereby fixed–free boundary conditions apply for the drivetrain torsion.
- The positive slip-torque slope (with or without hysteresis) in an asynchronous generator used in ASR turbines adds damping to modes involving drivetrain torsion, e.g. collective rotor modes and tower bending modes.

Recommendations for ASR turbines

- An aeroelastic stability tool that includes the positive damping of drivetrain rotational vibrations from the slip-torque relation of the asynchronous generator should be used in the assessment of the aeroelastic stability limits of ASR turbines.

References

[1] T. Buhl, K. Thomsen, and H. Markou. Design guidelines for integrated aeroelastic control of wind turbines – task-12 report. Technical Report Risø–R–1577(EN), Risø National Laboratory, Roskilde, Denmark, December 2006.

[2] E.S. Politis, J.G. Holierhoek, D. Winkelaar, T.G. van Engelen, V. Riziotis, S. Voutsinas, T. Buhl, H. Markou, K. Thomsen, M.H. Hansen, and S. Streiner. Parameter variations for active-stall and pitch-regulated turbine – task-6 report. Technical Report Risø-I-2413(EN), Risø National Laboratory, 2005.

[3] H. Stiesdal. Extreme wind loads on stall regulated wind turbines. *In Proceedings of the 16th British Wind Energy, Association Conference, El-liot G (ed.). Mechanical Engineering Publications Limited: London*, pages 101–106, 1994.

[4] K. Thomsen, J.T. Petersen, E. Nim, Øye, and B. S., Petersen. A method for determination of damping for edgewise blade vibrations. *Wind Energy*, 3:233–246, 2001.

[5] F. Rasmussen, J.T. Petersen, D. Winkelaar, and R. Rawlinson-Smith. Response of stall regulated wind turbines - stall induced vibrations. Technical Report Risø-R-691(EN), Risø National Laboratory, Roskilde, Denmark, June 1993.

[6] J. T. Petersen, H. Aa. Madsen, A. Björck, P. Enevoldsen, S. Øye, H. Ganander, and D. Winkelaar. Prediction of dynamic loads and induced vibrations in stall. Technical Report Risø-R-1045(EN), Risø, Roskilde, Denmark, May 1998.

[7] F. Rasmussen, J.T. Petersen, and H.Aa. Madsen. Dynamic stall and aerodynamic damping. *Journal of Solar Energy Engineering*, 121:150–155, 1999.

[8] A. Björck, J. Dahlberg, Östman, and H. A., Ganander. Computations of aerodynamic damping for blade vibrations in stall. *European Wind Energy Conference, Dublin*, pages 503–507, 1997.

[9] P.K. Chaviaropoulos. Flap/lead–lag aeroelastic stability of wind turbine blades. *J. Wind Energy*, 4(4):183–200, 2001.

[10] M.H. Hansen. Improved modal dynamics of wind turbines to avoid stall-induced vibrations. *Wind Energy*, 6:179–195, 2003.

[11] M.H. Hansen. Aeroelastic stability analysis of wind turbines using an eigenvalue approach. *Wind Energy*, 7:133–143, 2003.

[12] D.W. Lobitz. Aeroelastic stability predictions for a mw-sized blade. *Wind Energy*, 7:211–224, 2004.

[13] D. W. Lobitz. Parameter sensitivities affecting the flutter speed of a MW-sized blade. *Journal of Solar Energy Engineering, Transactions of the ASME*, 127(4):538–543, 2005.

[14] M. H. Hansen. Stability analysis of three-bladed turbines using an eigenvalue approach. In *2004 ASME Wind Energy Symposium*, pages 192–202, Reno, January 2004.

[15] T. Burton, D. Sharpe, N. Jenkins, and E. Bossanyi. *Handbook of Wind Energy*. John Wiley & Sons, 2001.

[16] W. H. Reed. Propeller-rotor whirl flutter: A state-of-the-art review. *Journal of Sound and Vibration*, 4(3):526–544, 1966.

[17] D. L. Kunz. Analysis of proprotor whirl flutter: Review and update. *Journal of Aircraft*, 42(1):172–178, 2005.

[18] D.C. Janetzke and K.R.V. Kaza. Whirl flutter analysis of a horizontal-axis wind turbine with a two-bladed teetering rotor. *Solar Energy*, 31(2):173–182, 1983.

[19] P. K. Chaviaropoulos, E. S. Politis, D. J. Lekou, N. N. Sorensen, M. H. Hansen, B. H. Bulder, D. Winkelaar, C. Lindenburg, D. A. Saravanos, T. P. Philippidis, C. Galiotis, M. O. L. Hansen, and T. Kossivas. Enhancing the damping of wind turbine rotor blades, the DAMPBLADE project. *Wind Energy*, 9(1-2):163–177, 2006.

[20] J. T. Petersen, K. Thomsen, and H. Aa. Madsen. Local blade whirl and global rotor whirl interaction. Technical Report Risø-R-1067(EN), Risø National Laboratory, Roskilde, Denmark, August 1998.

[21] R. L. Bisplinghoff, H. Ashley, and R. L. Halfman. *Aeroelasticity*. Dover Publications, 1955.

[22] Y. C. Fung. *An Introduction to the Theory of Aeroelasticity*. John Wiley & Sons, Inc., 1955. (Dover edition, 1993).

[23] L. Meirovitch. *Methods of Analytical Dynamics*. McGraw-Hill, 1970.

[24] T. J. Larsen, A. M. Hansen, and T. Buhl. Aeroelastic effects of large blade deflections for wind turbines. In *Proceedings of The Science of Making Torque from Wind*, pages 238–246, The Netherlands, April 2004. Delft University of Technology.

[25] A. Ahlström. Influence of wind turbine flexibility on loads and power production. *Wind Energy*, 9:237–249, 2006.

[26] H. Aa. Madsen and F. Rasmussen. A near wake model for trailing vorticity compared with the blade element momentum theory. *Wind Energy*, 7:325–341, 2004.

[27] H. Snel and J. G. Schepers. Joint investigation of dynamic inflow effects and implmentation of an engineering method. Technical Report ECN-C–94-107, Netherlands Energy Research Foundation ECN, Petten, Netherlands, April 1995.

[28] V.A. Riziotis and S.G. Voutsinas. Advanced aeroelastic modelling of complete wind turbine configurations in view of assessing stability characteristics. In *Proceedings of the European Wind Energy Conference 2003*, pages 46–51, Athens, Greece, March 2006.

[29] M. H. Hansen, P. Fuglsang, T. Thomsen, and T. Knudsen. Two methods for estimating aeroelastic damping of operational wind turbine modes from experiments. *Wind Energy*, 9(1-2):179–191, 2006.

[30] T. J. Larsen, M. H. Hansen, and F. Iov. Generator dynamics in aeroelastic analysis and simulations. Technical Report Risø–R–1375(EN), Risø National Laboratory, Roskilde, Denmark, July 2003.

A Whirl flutter model

This appendix contains the derivation of a two degrees of freedom model used for the whirl flutter analysis in Section 6.1 with the assumptions listed in that section.

The equations of motions for the tilt θ and yaw υ degrees of freedom about the pivot point at the tower top (see schematics in Figure 19) can be written as

$$I\ddot{\upsilon} + J\Omega\dot{\theta} + k_\upsilon \upsilon = M_\upsilon \;\text{ and }\; I\ddot{\theta} - J\Omega\dot{\upsilon} + k_\theta\theta = M_\theta \tag{A.4}$$

where I is the moment of inertia of the nacelle and rotor for tilt and yaw about the pivot point, J is the azimuthal moment of inertia of the rotor and drivetrain, Ω is the rotor speed, k_υ and k_θ are the tilt and yaw stiffnesses at the pivot point, and $\dot{(\,)} = d/dt$ denotes differentiation with respect to time.

The aerodynamic moments in tilt M_θ and yaw M_υ are derived as the generalized forces for the tilt and yaw degrees of freedom due to the thrust T_i and torque Q_i forces summarized over all three blades and integrated over the blade span [23]:

$$M_\upsilon = \sum_{i=1}^{3} \int_0^R \frac{\partial \mathbf{r}_i}{\partial \upsilon} \cdot \mathbf{F}_i \, dr \;\text{ and }\; M_\theta = \sum_{i=1}^{3} \int_0^R \frac{\partial \mathbf{r}_i}{\partial \theta} \cdot \mathbf{F}_i \, dr \tag{A.5}$$

where $\mathbf{r}_i$ is the vector from the pivot point to the radial section on blade number i with the aerodynamic forces given by the vector $\mathbf{F}_i$. These vectors can be written as

$$\mathbf{r}_i = \mathbf{T}\,\{0, -l, r\}^T \;\text{ and }\; \mathbf{F}_i = \mathbf{T}\,\{Q_i, T_i, 0\}^T \tag{A.6}$$

where l is the distance from the pivot point to the rotor center, and r is the radial distance from rotor center to the blade section. The transformation matrix $\mathbf{T} = \mathbf{T}(\upsilon, \theta, \psi_i)$ handles the azimuthal rotation of the blade (cf. Figure 19) is:

$$\mathbf{T} = \cos\psi_i \mathbf{I} + \sin\psi_i \left[\mathbf{n} \times \mathbf{e}_1 \;\; \mathbf{n} \times \mathbf{e}_2 \;\; \mathbf{n} \times \mathbf{e}_3\right] + (1 - \cos\psi_i)\, \mathbf{n}\,\mathbf{n}^T \tag{A.7}$$

where $\psi_i = \Omega t + 2\pi(i-1)/3$ is the azimuth angle of blade number i, $\mathbf{e}_j$ are the unit vectors of the inertia system, and $\mathbf{n} = \{-\sin\upsilon, 1, \sin\theta\}^T/(3 - \cos^2\upsilon - \cos^2\theta)$ is a normalized vector along the shaft of rotation which tilts and yaws with the nacelle.

The local thrust and torque forces (without blade number indices) are given by

$$\begin{aligned} T &= \tfrac{1}{2}\rho c U^2 \left(C_L(\alpha)\cos\phi + C_D(\alpha)\sin\phi\right) \\ Q &= \tfrac{1}{2}\rho c U^2 \left(C_L(\alpha)\sin\phi - C_D(\alpha)\cos\phi\right) \end{aligned} \tag{A.8}$$

where ρ is the air density, c is the local chord length, and $C_L(\alpha)$ and $C_D(\alpha)$ are the lift and drag coefficients at the local angle of attack α. The local relative inflow velocity U, inflow angle ϕ, and angle of attack α are derived from the axial and tangential components of the local velocity triangle:

$$\phi = \arctan u_a/u_t \;, \;\; \alpha = \phi - \theta_0 \;\text{ and }\; U^2 = u_a^2 + u_t^2 \tag{A.9}$$

where θ_0 is the local twist of the blade chord. These components of the local velocity triangle (cf. Figure 19) on blade number i are derived as [18]:

$$\begin{aligned} u_a &= U_{a_0}\cos\upsilon\cos\theta + r\left(\dot{\theta}\cos\psi_i - \dot{\upsilon}\sin\psi_i\right) \\ u_t &= U_{t_0} - U_{a_0}\left(\cos\theta\sin\upsilon\cos\psi_i + \cos\upsilon\sin\theta\sin\psi_i\right) + l\left(\dot{\theta}\sin\psi_i + \dot{\upsilon}\cos\psi_i\right) \end{aligned} \tag{A.10}$$

where $U_{a_0} = U_0\sin\phi_0$ and $U_{t_0} = U_0\cos\phi_0$ are the axial and tangential components of the steady state inflow (including induced velocities) with mean relative velocity U_0 and inflow angle to rotor plane ϕ_0 at the radial section r.

Substitution of the local velocity components (A.10), the local flow relations (A.9), the local thrust and torque forces (A.8) into the aerodynamic tilt and yaw moments (A.5), and linearization by Taylor expansion for small tilt and yaw motions $\theta, \upsilon << 1$, these moments can be written as

$$\begin{aligned} M_\upsilon &= -k_{11}\upsilon + k_{21}\theta - c_{11}\dot{\upsilon} - c_{12}\dot{\theta} \\ M_\theta &= -k_{21}\upsilon - k_{11}\theta + c_{12}\dot{\upsilon} - c_{11}\dot{\theta} \end{aligned} \tag{A.11}$$

where the trigonometric relations $\sum_{i=1}^{3}\cos\psi_i = \sum_{i=1}^{3}\sin\psi_i = \sum_{i=1}^{3}\cos\psi_i\sin\psi_i = 0$ and $\sum_{i=1}^{3}\cos^2\psi_i = \sum_{i=1}^{3}\sin^2\psi_i = 3/2$ have been used, and the coefficients are

$$\begin{aligned} k_{11} &= \frac{3\rho l}{4}\int_0^R cU_0^2\sin\phi_0\left((C_L + C'_D)\cos\phi_0\sin\phi_0 + (C_D - C'_L)\sin^2\phi_0 - 2C_D\right)dr \\ &+ 3\rho l\int_0^R cU_0^2\left(C_L\cos\phi_0 + C_D\sin\phi_0\right)dr \\ k_{21} &= \frac{3\rho}{4}\int_0^R cU_0^2\sin\phi_0\left((C_L + C'_D)\sin^2\phi_0 + (C'_L - C_D)\cos\phi_0\sin\phi_0 - 2C_L\right)rdr \\ &+ \frac{3\rho}{2}\int_0^R cU_0^2\left(C_L\sin\phi_0 - C_D\cos\phi_0\right)rdr \\ c_{11} &= \frac{3\rho}{4}\int_0^R cU_0\left((C'_L - C_D)\cos^2\phi_0 + (C_L + C'_D)\cos\phi_0\sin\phi_0 + 2C_D\right)r^2dr \\ &+ \frac{3\rho l^2}{4}\int_0^R cU_0\left((C'_L - C_D)\sin^2\phi_0 - (C_L + C'_D)\cos\phi_0\sin\phi_0 + 2C_D\right)dr \\ c_{12} &= -\frac{3\rho l}{4}\int_0^R cU_0\left(3C_L - C'_D\right)rdr \end{aligned} \tag{A.12}$$

where the aerodynamic coefficients C_L and C_D, and their derivatives C'_L and C'_D are evaluated at the mean angle of attack $\alpha_0 = \phi_0 - \theta_0$.

The linearized aerodynamic tilt and yaw moments (A.11) have a symmetric part given by the aerodynamic stiffness and damping coefficients k_{11} and c_{11}, and a skew-symmetric part given by the aerodynamic stiffness and damping coefficients k_{21} and c_{12}. The coefficients depend on the air density ρ, the rotor tip radius R, the distance from the pivot point to the rotor center l, and the radial distributions of chord length c, mean relative inflow velocity U_0, mean inflow angle ϕ_0, and mean angle of attack α_0 determining the aerodynamic lift and drag coefficients and their derivatives.

The symmetric stiffness coefficient is positive $k_{11} > 0$, mainly because the thrust on the rotor T has the linearized components $-2lT\theta$ and $-2lT\upsilon$ in the tilt and yaw directions. If the pivot point is placed at the rotor center $l = 0$ then the symmetric stiffness vanish $k_{11} = 0$. The skew-symmetric stiffness coefficient is positive $k_{21} > 0$ mainly because the torque on the rotor Q has the components $-Q\upsilon$ and $Q\theta$ in the tilt and yaw directions.

The symmetric damping coefficient is positive $c_{11} > 0$ for attached flow on the outer part of the rotor where the aerodynamic coefficients and their gradients are positive $C_L, C_D, C'_L, C'_D > 0$ with $C'_L >> C_D$ and noting that $l < R$ and $0 < \phi_0 < \pi/2$. In fact, the symmetrical term is large for attached flow, whereby the structural damping of tilt and yaw motion will have insignificant effect on the whirl flutter limits. The skew-symmetric damping coefficient is negative $c_{12} < 0$ for attached flow on the outer part of the rotor where $C_L > C'_D > 0$.

Figure 20 shows the chord distribution, inflow conditions and aerodynamic coefficients along the blade for NM80 turbine at 20 m/s extracted from the nonlinear simulation tool

used for the whirl flutter analysis in Section 6.1. From these parameters, the spanwise distribution of the aerodynamic moment coefficients are derived from Equation (A.12) and shown in the lowest plot. The integrated coefficients and the other parameters of the simple model are listed in Table 1.

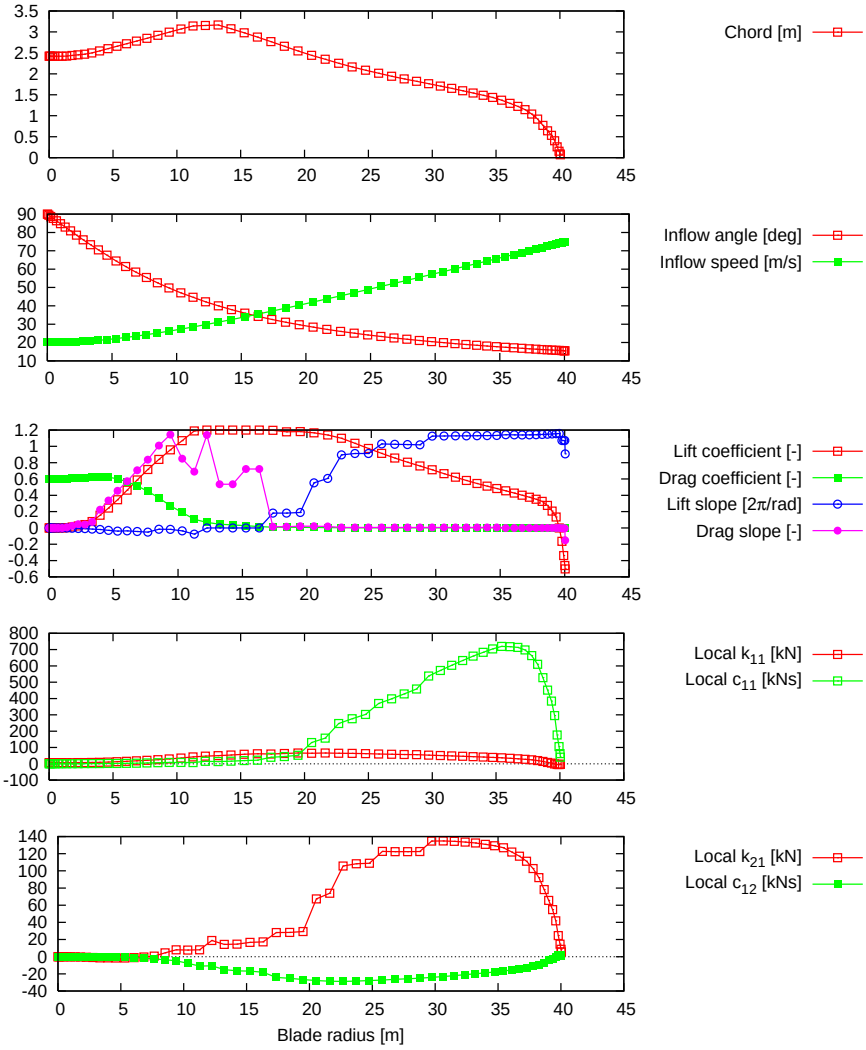

Figure 27. Chord distribution, inflow conditions and aerodynamic coefficients along the blade for NM80 turbine at 20 m/s extracted from the nonlinear simulation tool, and the spanwise distribution of the aerodynamic coefficients derived from Equation (A.12).

Parameter	Value	
R	40.04	m
l	4.03	m
I	5.45	Gg m^2
J	8.97	Gg m^2
Ω	1.8	rad/s
ρ	1.25	kg/m^3
k_{11}	1.64	MNm/rad
k_{21}	2.41	MNm/rad
c_{11}	9.63	MNms/rad
c_{12}	-0.62	MNms/rad

Table 1. System parameters and aerodynamic coefficients are computed for the NM80 turbine at 20 m/s (cf. Figure 27).

Risø's research is aimed at solving concrete problems in the society.

Research targets are set through continuous dialogue with business, the political system and researchers.

The effects of our research are sustainable energy supply and new technology for the health sector.